Chemical Society Review

REVIEW

Double-Cavity Cucurbiturils: Synthesis, Structures, Properties, and Applications

Received 00th January 20xx,
Accepted 00th January 20xx

DOI: 10.1039/x0xx00000x

www.rsc.org/

Zhengwei Yu,[a] Qing Li,*[a] Carl Redshaw,[b] Xin Xiao*[a] and Zhu Tao*[a]

Double-cavity Q[*n*]s are relatively new members of the Q[*n*] family and have garnered significant interest due to their distinctive structures and novel properties. While they incorporate n glycoluril units, akin to their single-cavity counterparts, their geometry can best be described as resembling a figure-of-eight or a handcuff, distinguishing them from the single-cavity Q[*n*]s. Despite retaining the core molecular recognition traits of single-cavity Q[*n*]s, these double-cavity variants introduce fascinating new attributes rooted in their distinct configurations. This overview delves into the synthesis, structural attributes, properties, and intriguing applications of double-cavity Q[*n*]s. Some of the applications explored include their role in supramolecular polymers, molecular machinery, supra-amphiphiles, sensors, artificial light-harvesting systems, and adsorptive separation materials. On conclusion this review, we discuss potential challenges and avenues for future development and offer valuable insights for other scholars working in this area with the aim of catalyzing further exploration and interest.

1. Introduction

The field of supramolecular chemistry owes its inception to the groundbreaking work of Lehn, Cram, and Pedersen, who collectively secured the 1987 Nobel Prize in Chemistry for their seminal contributions.[1] In the ensuing years, there has been a proliferation of studies focused on the fundamental science underpinning noncovalent interactions and the self-assembly processes[2] paving the way for the creation of functional supramolecular systems. These systems have found a myriad applications, ranging from chemical sensors,[3,4] imaging agents,[5] separation materials,[6,7] and molecular machines.[8,9] Beyond these, they have also marked their presence in various biomedical domains.[10] Macrocyclic hosts, such as crown ethers,[11–15] cyclodextrins,[16–20] calixarenes,[21–24] cucurbiturils,[25–31] and pillararenes,[32–37] have played a key role in the development of supramolecular chemistry. Over the recent two decades, these hosts have found utility in the construction of molecular machines,[38,39] targeted drug-delivery systems,[40–43] advanced adsorptive separation materials,[44–47] and adaptive supramolecular polymers.[48–53] Furthermore, they have been integral to the development of stimuli-responsive molecular recognition processes.[54,55]

Cucurbit[*n*]urils (Q[*n*] or CB[*n*], *n* = 5–8, 10; Fig. 1) are a class of macrocyclic hosts comprising *n* glycoluril units linked by 2*n* CH_2-bridges and a single hydrophobic cavity flanked by electrostatically negative ureidyl C=O portals. Although cucurbit[6]uril was first reported by Behrend *et al.* in 1905,[56] its chemical structure was not elucidated until 1981 by Mock *et al.*[57] Around the turn of the millennium, the Q[*n*] family was expanded to include Q[*n*] homologs (Q[5], Q[7], Q[8], and Q[10]) with only a single cavity.[51,58–61] To date, hundreds of Q[*n*]-type receptors have been synthesized, their fundamental molecular recognition properties explored, and their applications developed. These hosts contain anywhere from four (*e.g.*, Me_8TD[4]) to 15 building blocks (twisted cucurbit[15]uril, *t*Q[15]).[51,58,60–70] The defining molecular recognition properties of Q[*n*] hosts include their high affinity and selectivity[62–67] toward hydrophobic dications in water, their constrictive binding, their high stimulus responsiveness (*e.g.*, pH, electrochemical, chemical, and photochemical), and the low polarizability of the Q[*n*] cavity.[29,30,55,68–71] Therefore, Q[*n*] have been effectively utilized to develop drug-delivery systems,[62,72,73] engage in biomolecular recognition,[74,75] create adsorptive separation materials,[76–80] fabricate supramolecular polymers,[81–85] and to establish chemical sensing ensembles.[86–88]

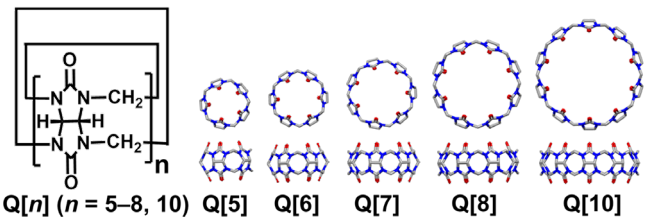

[a] Key Laboratory of Macrocyclic and Supramolecular Chemistry of Guizhou Province, Institute of Applied Chemistry, Guizhou University, Guiyang 550025, P. R. China
[b] Chemistry, School of Natural Sciences, University of Hull, Hull HU6 7RX, U.K.

Fig. 1 General chemical structure and X-ray crystal structures of Q[*n*]s (*n* = 5–8, 10).

Double-cavity Q[*n*]s are distinguished not only by their novel structures but, more significantly, by their unique properties. The Isaacs group, since 2006, has systematically synthesized and identified a range of double-cavity Q[*n*]s using controlled methodologies. This series includes *nor-seco*-cucurbit[10]uril (*bis-ns*-Q[10]),[89] an imidazolidone derivative of *bis-ns*-Q[10] (IM-*bis-ns*-Q[10]),[90] acyclic glycoluril decamer ((±)-AGD),[91] two dimeric cucurbit[6]urils (Q[6]–Q[6]1 and Q[6]–Q[6]2),[92] and a cucurbit[6]uril–cucurbit[7]uril heterodimer (Q[6]–Q[7]).[93] Moreover, from 2013 onward, our group has brought to light a series of twisted cucurbit[*n*]urils: twisted cucurbit[13]uril (*t*Q[13]),[94] twisted cucurbit[14]uril (*t*Q[14]),[95] and twisted cucurbit[15]uril (*t*Q[15]) (Fig. 2).[94] Because of the double cavities, these Q[*n*]s usually not only exhibit differences from single-cavity Q[*n*]s in their host–guest interactions and the accompanying properties,[89,91,94,95] but also show that they are more capable of forming supramolecular frameworks than the single-cavity Q[*n*]s;[50,92,93] specifically, from the structural point of view, twisted Q[*n*]s should also be considered chiral.[94,95] Although double-cavity Q[*n*]s only account for a small part of the Q[*n*] family, many studies have been reported on their novel structures and special properties. However, to date, a summary of the double-cavity Q[*n*]s has not yet appeared in the literature. Therefore, this review outlines double-cavity Q[*n*]s, and discusses their synthesis, structures, properties, and main applications. On this basis, the possible challenges and future development directions are predicted. The provision of the references herein will help stimulate further research interest.

This review exclusively focuses on double-cavity Q[*n*]s, and we have deliberately excluded polymeric systems composed of multiple Q[*n*] units as they have been extensively discussed in previous reviews.[29,30,55,62,63,70,71]

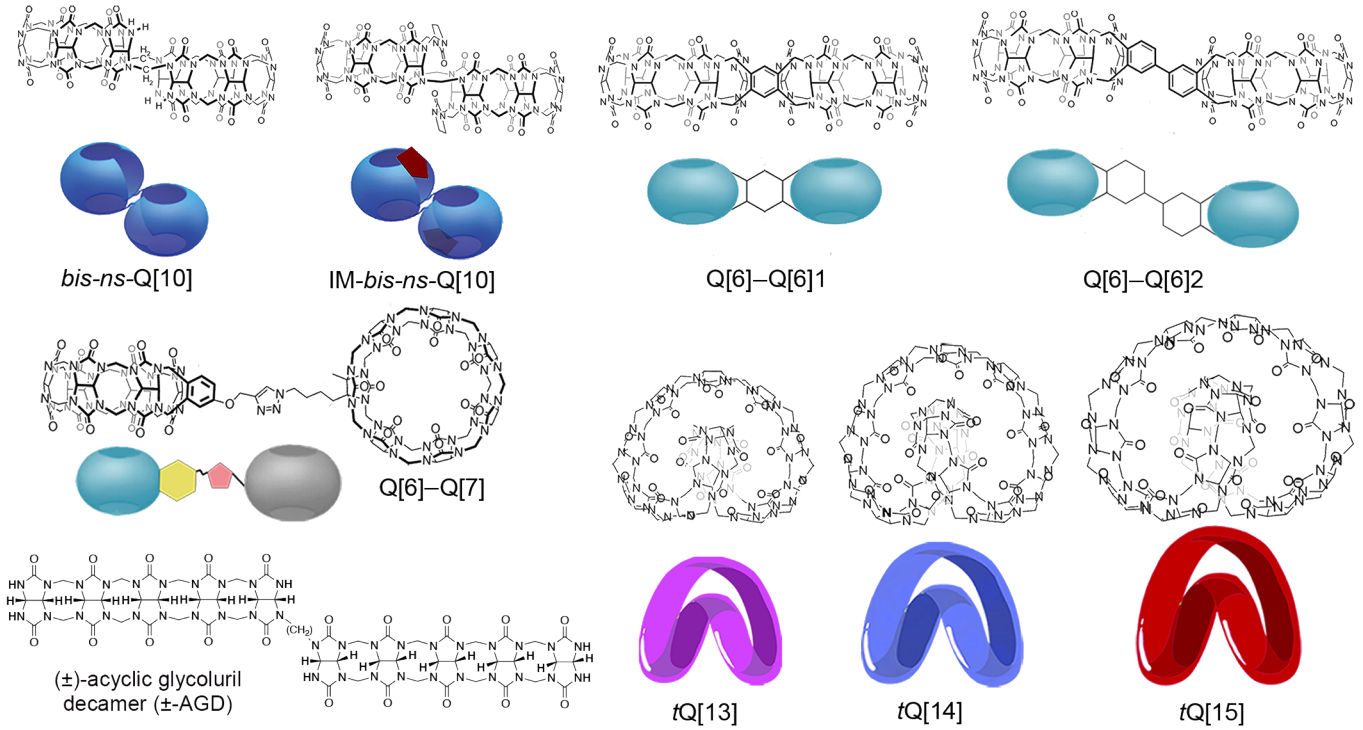

Fig. 2 Chemical structure of cucurbiturils featuring double cavities and their corresponding schematic representations.

2. Syntheses and Structures

The name "cucurbituril" derives from the resemblance of the single-cavity Q[*n*]s to the segmented shape of pumpkins which belong to the cucurbitaceae family of plants.[57] In contrast, double-cavity Q[*n*]s, despite incorporating glycoluril segments, possess intricate configurations that are reminiscent of handcuffs or the numeral 8, as depicted in Fig. 2.

In 2006, the Isaacs group reported a two-cavity Q[*n*], *bis-ns*-Q[10].[89] This compound can be accessed in 15% yield via the reaction of glycoluril and paraformaldehyde, followed by purification steps such as washing and recrystallization. Structurally, *bis-ns*-Q[10] encompasses two glycoluril pentamers connected by two methylene bridges (Fig. 2). In contrast to Q[10], *bis-ns*-Q[10] lacks the two CH_2-bridges and instead features two symmetrically equivalent cavities. These twin cavities are intimately connected, overlap slightly, and their dimensions are comparable to those of Q[6] and Q[7]. Molecular dynamic (MD) simulations revealed the four internal distances (Å) of *bis-ns*-Q[10] (d1 = 5.72 Å, d2 = 18.41 Å, d3 = 10.12 Å, and d4 = 10.12 Å, Fig. 3).[96] Furthermore, *bis-ns*-Q[10] exhibits two distinct C=O portals; one with a CH_2-bridge and the

other without this bridge. Interestingly, the cavities of *bis-ns*-Q[10] are only partially pre-organized and exhibit adaptability, altering their size and shape, both inherently and in the presence of guest molecules of varying sizes. The Isaacs group also reported (±)-AGD, isolated by ion-exchange chromatography from a reaction mixture containing glycoluril (1 eq.) and formaldehyde (1.67 eq.). (±)-AGD is chiral and racemic owing to its single CH_2-bridge between its two methylene-bridged glycoluril pentamer units (Fig. 2).[91] (±)-AGD becomes formally related to *bis-ns*-Q[10] when one CH_2-bridge is removed.

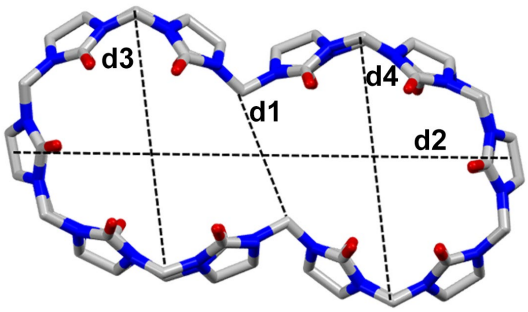

Fig. 3 Internal diameters of *bis-ns*-Q[10].

Moreover, the Isaacs group also reported IM-*bis-ns*-Q[10].[90] They heated *bis-ns*-Q[10] with formaldehyde and imidazolidone in 8 M hydrochloric acid (HCl) to obtain the IM-*bis-ns*-Q[10] precipitate in 78% yield. IM-*bis-ns*-Q[10] contains two imidazolidone units that bridge the NH groups at the position where the CH_2 groups of *bis-ns*-Q[10] are missing (Fig. 2). The carbonyl group of the imidazolidone units point toward the central CH_2-bridge, with a C=O···CH_2 distance of 2.35 Å. The distance between the two central CH_2-groups of IM-*bis-ns*-Q[10] is 4.5 Å less than that of *bis-ns*-Q[10]. Its average entry diameter is 6.9 Å, similar to that measured for Q[6]. Overall, the structure of IM-*bis-ns*-Q[10] is similar to that of *bis-ns*-Q[10]. Nevertheless, the bridging imidazolidones make the structure more rigid, bringing each cavity of IM-*bis-ns*-Q[10] closer to Q[6] in terms of size.[90]

The Isaacs group washed the insoluble precipitate obtained from the reaction of benzene-1,2,4,5-tetracarbaldehyde (1 eq.) and glycoluril hexamer (2 eq.) with methanol to isolate Q[6]–Q[6]1 in 30% yield. It can be deduced from the structure of Q[6]–Q[6]1 (Fig. 2) that it contains a benzene covalently linked to two glycoluril hexamers. The shape resembles two Q[6]s connected by covalent bonds. Each cavity of Q[6]–Q[6]1 has similar recognition properties to those of Q[6]. However, it is unfortunate that no additional information about the structure of Q[6]–Q[6]1 has been reported. DOWEX ion-exchange column chromatography and recrystallization was used to isolate pure Q[6]–Q[6]2 in 34% yield from the reaction mixture of biphenyl-3,3',4,4'-tetraacetaldehyde (1 equiv.) and glycoluril hexamer (2 equiv.). Structurally, Q[6]–Q[6]2 is obtained by combining two glycoluril hexamers with biphenyl (Fig. 2). The shape also resembles that of two Q[6]s connected by covalent bonds. The crystal structure of Q[6]–Q[6]2 shows that its biphenyl units exhibit a torsion angle of 36°, and that the Q[6] cavity displays a clear cavity ellipsoidal deformation (a = 10.8 Å, b = 9.3 Å, and c = 9.2 Å).[92] The same group prepared a Q[6]–Q[7] heterodimer by a click reaction of a preformed macrocyclic Q[7]-azide[97] and propargyloxy-Q[6][98,99] units. By using DOWEX ion-exchange column chromatography to purify the reaction mixture, Q[6]–Q[7] was produced in 17% yield. Q[6]–Q[7] is structurally composed of a Q[6] and a Q[7] linked by covalent bonds (Fig. 2). Although the crystal structure of Q[6]–Q[7] has not yet been reported, each cavity retains the innate binding ability of the parent Q[6] or Q[7] macrocycles.

Our group reported a unique class of twisted double-cavity Q[*n*]s (*t*Q[*n*], *n* = 13, 14, 15).[94,95] To synthesize *t*Q[14], glycoluril (0.35 mol), paraformaldehyde (0.86 mol), and HCl (100 mL, 12 mol/L) were heated and stirred to obtain a crude solid. Next, purification was performed on a DOWEX 50W × 2–400 (H) column to obtain *t*Q[14] as a white solid (1.2% yield). The synthetic process for *t*Q[13] and *t*Q[15] is similar to that of *t*Q[14]. Glycoluril (3.5 mol), paraformaldehyde (8.6 mol), and HCl (1000 mL, 12 mol/L) were heated to obtain a crude solid. When the purification was performed on a DOWEX 50W × 2–400 (H) column and silica gel plate, *t*Q[13] (0.2% yield), *t*Q[14] (3% yield), and *t*Q[15] (0.6% yield) were obtained. Hosts *t*Q[13], *t*Q[14], and *t*Q[15] contain 13–15 glycoluril units, respectively, linked by 26–30 CH_2 bridges with a helically twisted figure-of-eight conformation, thus forming two cavities (Fig. 2). It can be seen from the crystal structures of *t*Q[13] and *t*Q[15][94] that they have the same shape as that of *t*Q[14] and differ structurally from *t*Q[14] by only one glycoluril unit. Given the similarity of *t*Q[*n*]s to each other, here we use a single crystal of *t*Q[14] complexed with Eu^{3+} as an example to further elucidate the structure of *t*Q[*n*]s. The X-ray crystal structure showed that *t*Q[14] has three carbonyl ports: Eu1 occupies two of the same ports, while Eu2 occupies the third port (Fig. 4a and b). The helically twisted figure-of-eight conformation of *t*Q[*n*]s is clearly depicted in Fig. 2. It is important to note that due to their helical structure, *t*Q[*n*]s are chiral, leading to the formation of enantiomers. *t*Q[*n*] can be viewed as a structure comprising two helices with the same pitch and opposite helical directions (Fig. 4); one of them is an outer helix with a bigger section, whereas the other is a central helix with a smaller section.[94] The helical structure of *t*Q[*n*] gives rise to a central cavity (green portion in Fig. 4c) formed by the central helix and two side cavities (yellow and blue parts of Fig. 4d) formed by the space between the central helix and the outer helix (center cavity and side cavities overlap spatially). Based on the crystal structure,[94,95] the central cavity volumes of *t*Q[13], *t*Q[14], and *t*Q[15] are calculated to be 70 ± 10 $Å^3$, 120 ± 30 $Å^3$, and 140 ± 30 $Å^3$, respectively, and the two identical side cavity volumes are 140 ± 20 $Å^3$, 200 ± 40 $Å^3$, and 250 ± 50 $Å^3$, respectively. The experimental data suggests that *t*Q[14] contains two distinct cavities characterized

by differing spatial environments, capable of encapsulating two or even three guest molecules possessing suitable shapes and sizes.[100]

The two cavities presented by the double-cavity Q[*n*] have unique shapes, a rare phenomenon in macrocyclic compounds that gives rise to numerous novel and unique properties and applications. In particular, due to the late discovery of *t*Q[13] and *t*Q[15], there are many research gaps that warrant further exploration.

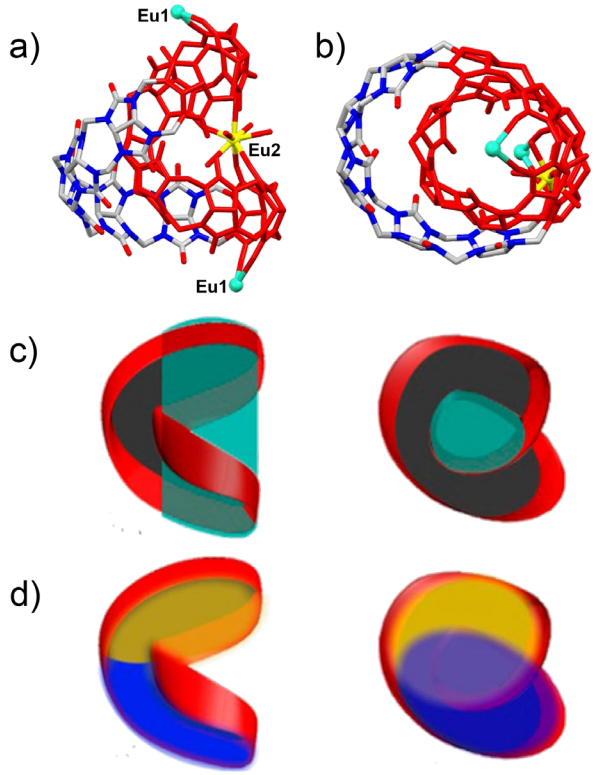

Fig. 4 X-ray crystal structure of the *t*Q[14]-Eu^{3+} complex: (a) side view and (b) top view; c) center cavity of *t*Q[*n*]; and d) side cavity of *t*Q[*n*]. Reproduced with permission from ref. 94. Copyright 2016, American Chemical Society.

3. Difference in the Properties of Double-Cavity Q[*n*]s and Traditional Single-Cavity Q[*n*]s

Although the cavity shapes of double-cavity Q[*n*]s differ from those of Q[5], Q[6], Q[7], Q[8], and Q[10], they preserve the fundamental molecular recognition properties of hosts in the Q[*n*] family. Theoretically, double-cavity Q[*n*]s can encapsulate the guests that traditional single-cavity Q[*n*]s can encapsulate, including hydrophobic cations, metal ions, organic small molecules, inorganic small molecules, inorganic anions, and so on.[29,30,55,70,71,89,101–104] Similar to traditional single-cavity Q[*n*]s, double-cavity Q[*n*]s also exhibit high selectivity,[103,105–107] high binding affinity,[106–108] and high stimulus responsiveness.[50,93,101,102] These essential molecular recognition properties of Q[*n*] have been reviewed in detail.[29,30,55,70,71] This section focuses on the novel properties of double-cavity Q[*n*]s that make them different from traditional single-cavity Q[*n*]s and provide a means to address new opportunities and challenges and thereby broaden their potential applications in different fields.

3.1 Structural flexibility

The cavities of traditional single-cavity Q[*n*]s are relatively rigid and display well-defined shapes and dimensions. In contrast, double-cavity Q[*n*] hosts *bis-ns*-Q[10], (±)-AGD, and *t*Q[14] are structurally flexible. The two cavities of *bis-ns*-Q[10 and *t*Q[14] are not independent; therefore, conformational changes in one cavity transmit and affect the size and shape of the other. Such unique structural features lead to some interesting observations.

For a more comprehensive insight into *bis-ns*-Q[10], after obtaining *bis-ns*-Q[10], the Isaacs group studied it in combination with some common Q[*n*] guests (alkylamines, cycloalkylamines, arylamines, adamantanes, ferrocenes, and viologens). They reported that *bis-ns*-Q[10] could form ternary complexes (*bis-ns*-Q[10]•$guest_2$) with smaller guests (alkylamines, cycloalkylamines, arylamines, and adamantanes) and binary complexes (*bis-ns*-Q[10]•guest) with a larger guest (viologens). However, the simultaneous presence of both ternary and binary complexes has never been observed, which suggests that this system exhibits considerable positive cooperativity.[89] To demonstrate this positive cooperativity, the Isaacs group inserted a mixture of two guests that differ in size in *bis-ns*-Q[10] and observed the preferential formation of a mixture of two homomeric ternary complexes when the sizes of the guests were significantly different (*e.g.*, *p*-xylene diamine *versus* dimethylaminomethyl ferrocene). However, when mixtures of similar-sized guests were used (*e.g.*, *p*-xylene diamine *versus* cystamine), a mixture of homomeric and heteromeric ternary complexes formed. These findings reveal that the binding of the first guest pre-organizes the second cavity to bind to a similarly sized guest. This flexible structural feature of *bis-ns*-Q[10] stems from the flexibility of the bridging methylene groups in its structure (Fig. 5a). Experimental and theoretical studies on the binding properties of *bis-ns*-Q[10] toward selected protonated alkyl and aryl amines were carried out by the Gerbaux group using mass spectrometry and computational chemistry.[109,110] They found that in the assembly of ternary complexes of *bis-ns*-Q[10], the binding of one ligand facilitates the complexation of another analogous ligand at the second binding site. The Assaf group investigated the structure and dynamics of inclusion complexes containing *bis-ns*-Q[10] as a host molecule with 1-adamantylmethylammonium (AH) as the guest molecule using MD simulations.[96] They performed MD simulations of 1:1 inclusion complexes of *bis-ns*-Q[10] with 1-adamantane methylamine in an aqueous solution. The results showed that the guest molecule in one of the cavities of *bis-ns*-

Q[10] complex induces an allosteric conformational change in the neighbouring empty cavity. The work of the Gerbaux group and the Assaf group verified the Isaacs group's conclusions about homotropic allostery.

Using DOWEX ion-exchange chromatography, the Isaacs group isolated (±)-AGD as a minor product of the reaction of glycoluril with a low amount of formaldehyde (1.67 eq.).[91] The ^{1}H NMR spectrum of (±)-AGD in 20% deuterium chloride was uninterpretable, although a clear singlet at 4.5 ppm was seen for the central CH_2 group. Upon adding excess sodium sulfate, large upfield shifts were observed in the ^{1}H NMR spectrum, indicating a conformational change and a self-assembly process. Fig. 5b shows the X-ray crystal structure of the (+)-AGD•(-)-AGD•$(Na^+)_6$ complex, which is a heterochiral dimer of decamers. The six sodium ions are seen to form C=O···Na^+ interactions with three or four ureidyl carbonyl groups, thereby neutralizing the high electrostatic potential of the portals and forming an assembly. The convex face of each AGD molecule weaves itself through the opposing cavity of AGD, driven in part by the hydrophobic effect.

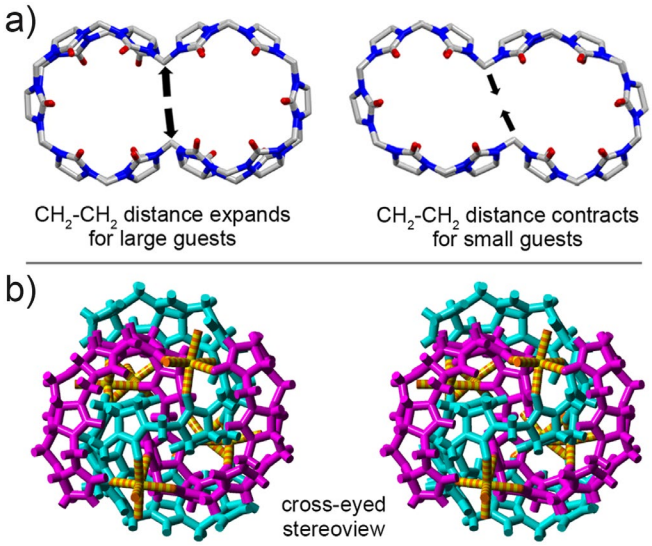

Fig. 5 a) Illustration of the conformational change upon binding different-sized guests to *bis-ns*-Q[10]; b) stereoview of the X-ray crystal structure of (+)-AGD•(-)-AGD•$(Na^+)_6$.

The *t*Q[14] host, which exhibits structural flexibility, displays quite interesting binding properties that are distinct from those of *bis-ns*-Q[10] described above. Our group found that samples prepared from single crystals of the Eu^{3+}-*t*Q[14] complex (Fig. 4a) exhibited an entirely different ^{1}H NMR spectrum (Fig. 6a) from that of *t*Q[14] alone (Fig. 6b).[95] Fig. 6c shows the ^{1}H NMR spectrum obtained upon adding $Eu(NO_3)_3$ to a D_2O solution of *t*Q[14] (Eu^{3+}/*t*Q[14] = 2), which is similar to that shown in Fig. 6a. Therefore, *t*Q[14] interaction with metal ions is accompanied by a structural transition which means *t*Q[14] can be highly flexible. Interestingly, *t*Q[14], which is soluble in water and organic solvents, exhibits different binding properties in different solvents and can accommodate 1 to 3 guests. Initially, *t*Q[14] was found to prefer to wrap the 4,4′-bipyridine moiety of the 1,6-di(4,4′-bipyridine) guest in DMSO-d_6, whereas the 4,4′-bipyridine moiety is located outside of the portal of *t*Q[14] in D_2O.[95] Motivated by the fact that the *t*Q[14]–guest binding situation would be different in water *versus* DMSO, our group further explored the interaction of *t*Q[14] with alkyl diammonium ions ($^+H_3N(CH_2)_nNH_3^+$, n = 2, 4, 6, 8, 10) in D_2O and DMSO-d_6.[100] The results showed that all alkyldiammonium guests can be encapsulated somewhere within the *t*Q[14]. The main drivers of the binding behaviour of *t*Q[14] with alkyldiammonium guests in aqueous solution are ion-dipole and hydrophobic interactions. However, in DMSO-d_6 media, alkyldiammonium guests cannot undergo significant hydrophobic interactions with *t*Q[14], and as a consequence, the ion-dipole interactions become the main drivers of host–guest complexation. Interestingly, the ^{1}H NMR spectrum integrals of *t*Q[14] and the interacted alkyl diammonium ions showed that *t*Q[14] can bind one, two, or even three guest molecules. For example, it can encapsulate two or three $^+H_3N(CH_2)_2NH_3^+$ or one or two $^+H_3N(CH_2)_nNH_3^+$ (n = 4 and 6). It must be noted that due to the limitations of the ^{1}H NMR spectra, more details concerning the interaction of *t*Q[14] with alkyl diammonium ions are not known. *t*Q[13] and *t*Q[15] are also soluble in water and organic solvents, suggesting that the solubility of *t*Q[*n*]s differs from that of conventional single-cavity Q[*n*]s. Moreover, although there is no data regarding the structural flexibility of *t*Q[13] and *t*Q[15], their conformational adaptability is probable given their structural resemblance to *t*Q[14].[94]

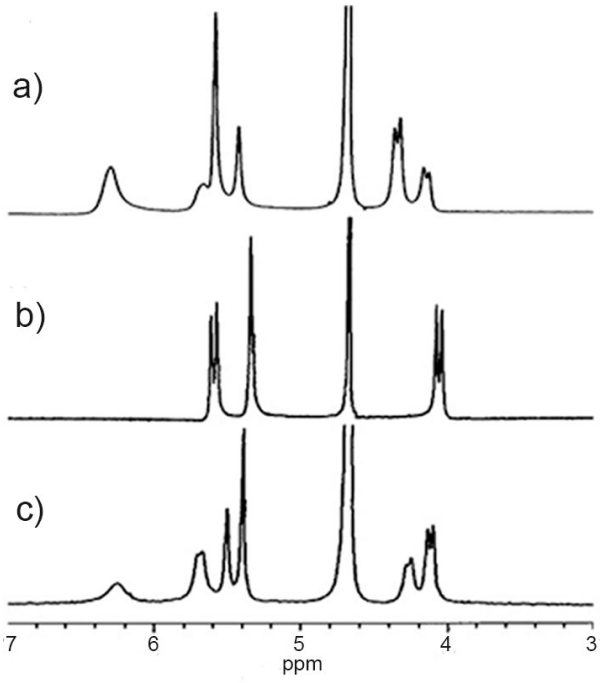

Fig. 6 ^{1}H NMR spectra (400 MHz, D_2O, 25 °C) of: a) single crystals of the Eu^{3+}-*t*Q[14] complex; b) *t*Q[14]; and c) *t*Q[14] in the presence of approximately 2.0 equiv. of $Eu(NO_3)_3$. Reproduced with permission

from ref. 95. Copyright 2013, Wiley-VCH Verlag GmbH & Co. KGaA, Weinheim.

In addition to being able to encapsulate one guest, double-cavity Q[*n*]s can also encapsulate two or even three guests that could be the same or different, a feature not commonly observed in conventional supramolecular hosts. Comprehending the spatial characteristics of the two cavities within double-cavity Q[*n*]s can help in expanding their applications, such as in biomimetic allosteric systems, the development of supramolecular polymers, and the creation of covalent multivalent Q[*n*] scaffolds. This phenomenon could lead to significant developments in the field of supramolecular chemistry.

3.2 Isomerism

Double-cavity Q[*n*]s can display interesting types of isomerism. *Bis-ns*-Q[10] has two types of C=O portals. Hence, when unsymmetrical ion guests are combined with *bis-ns*-Q[10], three diastereoisomers can be formed depending on where the guest is located, namely top–top, center–center, and top–center (Fig. 7) forms.[89] These three isomers can be illustrated using *bis-ns*-Q[10]•$(AH)_2$ complex as an example. The top–top configuration is obtained when the NH_3^+ groups bind at the ports lacking a CH_2-bridge. When the NH_3^+ groups bind at the ports containing a CH_2-bridge, the configuration becomes center–center. When one NH_3^+ group binds at the port lacking a CH_2-bridge and the other at the ports containing a CH_2-bridge, the configuration is top–center. The ability of *bis-ns*-Q[10] to form ternary complexes with smaller guests (*e.g.*, AH) is the key to producing the abovementioned three isomers. The Assaf group studied the structure and kinetics of 1:1 and 1:2 inclusion complexes formed by *bis-ns*-Q[10] with AH using MD simulations in water.[96] They found that the main contribution to the binding free energy (ΔG) of each isomer comes from the host–guest electrostatic interaction. In both 1:1 and 1:2 complexes, the ammonium group of AH interacted with the oxygen of the carbonyl group through ionic dipole interactions and hydrogen bonding, while it's hydrophobic part was located in the cavity of the host. The analyses of average structure and hydrogen bonding indicated that the ammonium group in the center orientation is more favorable to interact with the carbonyl entrance compared to the ammonium group in the top orientation. Electrostatic interaction energy (ΔE_{elec}) values obtained for the center orientation are also larger than those obtained for the top orientation. In addition, the additional ion dipole interaction between the second ammonium group and the carbonyl portal of the second cavity makes the ΔE_{elec} value of the 1:2 complex higher than that of the 1:1 complex. Finally, the ΔG values obtained for the 1:2 complexes ($\Delta G_{top-top}$ = −21.5 kcal/mol, $\Delta G_{top-center}$ = −26.8 kcal/mol, and $\Delta G_{cen-center}$ = −28.9 kcal/mol) and the 1:1 complexes (ΔG_{top} = −13.1 kcal/mol and ΔG_{center} = −17.1 kcal/mol) showed that the center–center 1:2 complex had the lowest ΔG, indicating that the center–center 1:2 complex was the most stable complex.

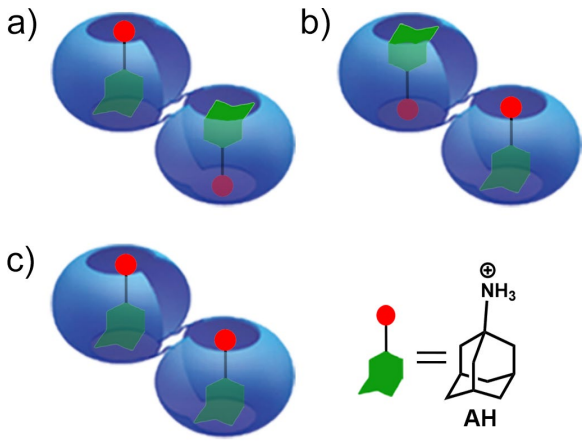

Fig. 7 Diastereomeric orientations of *bis-ns*-Q[10]•$(AH)_2$: a) top–top, b) center–center, and c) top–center.

Twisted *t*Q[*n*] hosts, with their structural helicity engendered by their 360° end-to-end twist along the C-shaped methylene-bridged glycoluril oligomer, exhibit chirality and exist as racemic mixtures of enantiomers.[94,95] The enantiomers of *t*Q[*n*]s are shown in Fig. 8. The structure of the *t*Q[*n*]s consists of covalently connected two helices of the same pitch but opposite helical directions.[94] This difference in helical orientation leads to the chirality of the *t*Q[*n*]s. Indeed, enantiomeric structures were observed in both crystal structures, one containing a complex of *t*Q[14] molecules and Dy^{3+} cations and the other comprising metal-free *t*Q[14] molecules, suggesting that chirality is an intrinsic property of *t*Q[14].[111] Therefore, *t*Q[13] and *t*Q[15] have inherent chirality because their structures are similar to that of *t*Q[14].[94]

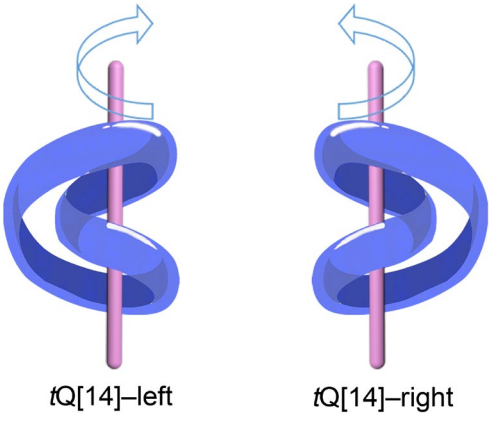

Fig. 8 Left- and right-handed forms of *t*Q[14].

The (±)-AGD complex, (+)-AGD•(-)-AGD•$(Na^+)_6$, obtained by the Isaacs group is also chiral.[91] This structure contains two (±)-AGD molecules with opposite handedness (Fig. 5b, purple and blue chains) that are integrated to produce the heterochiral

dimer, with the two helices screwed together at right angles to each other.

The isomerization of *bis-ns*-Q[10] is relatively well studied; however, this is not the case for *t*Q[*n*]s and (±)-AGD. For example, the method to obtain the left- and right-handed *t*Q[*n*]s has not yet been established, and their host–guest chemical properties are highly anticipated. Inducing the enantiomeric separation of double-cavity Q[*n*]s through interactions between a chiral guest and the double-cavity Q[*n*]s represents a viable and promising methodology. However, these aspects require further exploration.

4. Supramolecular Polymers

Supramolecular polymers are assemblies of monomers interconnected through noncovalent interactions. In recent years, Q[*n*]-based supramolecular polymers have been widely used in many fields.[48–53] Since their discovery, the double-cavity Q[*n*]s have been employed to construct supramolecular polymers with different geometrical features and properties. For example, the structures of double-cavity Q[*n*]s can be changed by varying their concentrations and using different exogenous compounds. Furthermore, double-cavity Q[*n*]-based supramolecular polymers can assemble via monomer units by noncovalent interactions in *n*-dimensional modes (such as linear, branching, and dendritic), thus allowing for various geometries. In this way, supramolecular polymers with varying properties have been successfully fabricated.

4.1 Supramolecular polymers based on *bis-ns*-Q[10]

The Isaacs group initially attempted to create supramolecular polymers by combining double-cavity *bis-ns*-Q[10]s with dimeric guests. However, low-molecular-weight cyclic 1:1 and 2:2 species were acquired.[105] The Zhang group[112] envisioned that linear supramolecular polymerization of guest monomers and *bis-ns*-Q[10] can be achieved by introducing Q[7] to the guest monomers through self-sorting. A bifunctional guest monomer (Naph-Phen-Naph), encompassing dual naphthalene (Naph) and one xylylene (Phen) binding sites, was synthesized to fabricate a supramolecular polymer by self-sorting amongst Naph-Phen-Naph, *bis-ns*-Q[10], and Q[7]. The naphthalene groups on both sides of Naph-Phen-Naph are capable of inserting into the two cavities of *bis-ns*-Q[10], serving as the driving force for the formation of supramolecular polymers. The Phen unit of Naph-Phen-Naph can be encapsulated in Q[7], which enhances the rigidity and orientation of the monomer. Ultimately, the Zhang group was able to avoid the two adverse factors that hinder supramolecular polymerization, namely dimerization and cyclization, through self-sorting of Naph-Phen-Naph, *bis-ns*-Q[10] and Q[7], and successfully constructed a high-molecular-weight supramolecular polymer comprising *bis-ns*-Q[10] (Fig. 9a). Interestingly, the molecular weight of the supramolecular polymer could be controlled by adjusting the molar ratio of Q[7]. The highest relative molecular mass (5.6×10^4 Da) of the supramolecular polymer (corresponding polymerization degree: ~16) was obtained when the molar ratio of Q[7] to Naph-Phen-Naph/*bis-ns*-Q[10] was 1.0. The relative molecular mass of the supramolecular polymer decreased from 5.6×10^4 to 1.4×10^4 Da when the molar ratio of Q[7] to Naph-Phen-Naph/*bis-ns*-Q[10] became more than 1.0. The decrease in molecular weight was due to the depolymerization of the supramolecular polymer caused by the binding of excess Q[7] to Naph as a competing host of *bis-ns*-Q[10]. These examples offer excellent demonstrations of how to prepare supramolecular polymers with varied topologies using self-sorting methods.

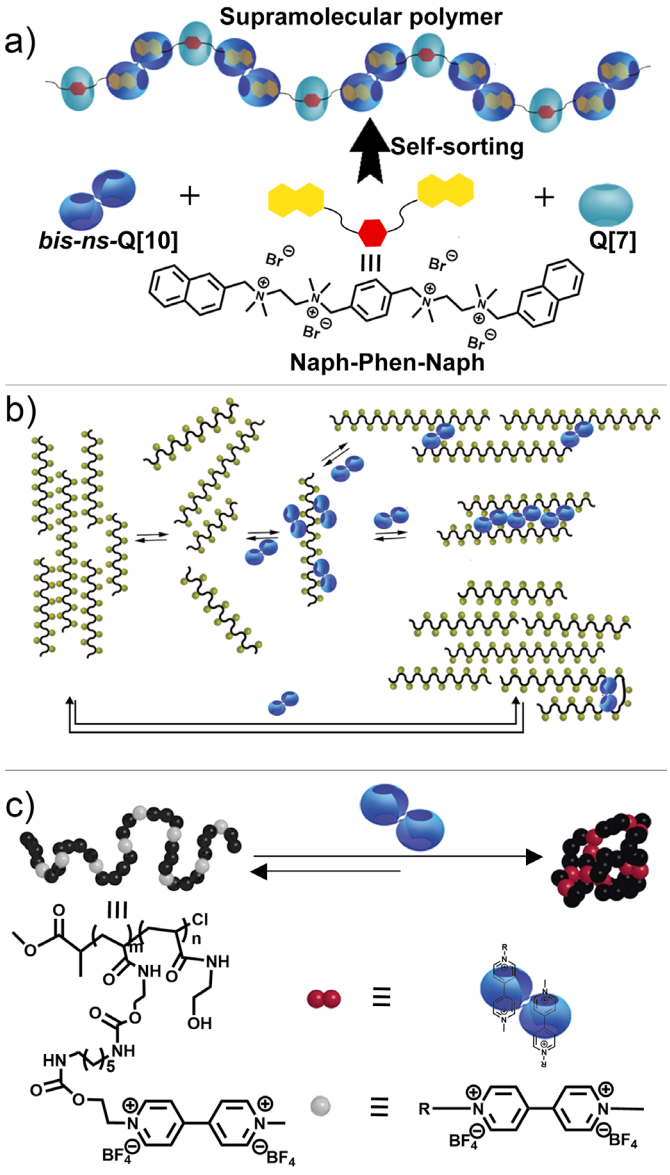

Fig. 9 a) Illustration of the self-sorting process to construct a supramolecular polymer; b) Possible equilibria among different morphologies of poly(diallyldimethylammonium chloride) in conjunction with *bis-ns*-Q[10]; c) Diagram showing the creation of

single-chain polymeric nanoparticles through a 2:1 complexation of MV with *bis-ns*-Q[10].

The Isaacs group also prepared supramolecular polymers using poly(diallyldimethylammonium chloride) and *bis-ns*-Q[10].[113] They found that the repeating units of the polymer chain bind within the two cavities of *bis-ns*-Q[10]. *Bis-ns*-Q[10] could complex both sides of the polymer chains through "cupping interactions". This phenomenon facilitated the bonding between individual polymer chains, which extended the polymer length (Fig. 9b). Moreover, the introduction of *bis-ns*-Q[10] into the solution of poly(diallyldimethylammonium chloride) decreased the relative viscosity. This occurred because the addition of *bis-ns*-Q[10] to the pre-prepared poly(diallyldimethylammonium chloride) solution disaggregated poly(diallyldimethylammonium chloride) and increased the length of the supramolecular polymer (Fig. 9b). These results also showed that the *bis-ns*-Q[10] assembly is reversible; thus, the external stimulus responsiveness of this system was examined. As this material exhibits potential sensitivity to external stimuli, it can be used in supramolecular photonics and electronics.

Scherman *et al*. reported metastable single-chain polymeric nanoparticles prepared through stimuli-responsive and reversible intramolecular cross-linking of an individual polymer chain in water (Fig. 9c).[114] They first prepared four poly(*N*-hydroxyethylacrylamide) polymers, and then bonded methyl viologen (MV), a good guest of *bis-ns*-Q[10], to the polymer chain to obtain new functional polymers with different molecular weights (168 kDa, 269 kDa, 291 kDa, and 492 kDa) and methyl viologen loadings (10%, 10%, 30%, and 10%). These MV functional groups can form 2:1 ternary host–guest complexes with *bis-ns*-Q[10], which allows individual polymer chains to 'collapse' and form nanoparticles. The reversible host–guest complexation between *bis-ns*-Q[10] and MV allows the transformation in a reversible supramolecular manner. The dynamic light scattering and atomic force microscopy measurements showed the formation of appropriately regulated structures. Interestingly, the particle size could be adjusted by changing the relative molecular mass of the polymer, such as loading the polymer chain with guest groups or changing the molecular weight of the initial polymer. More importantly, the particle size also can be adjusted by adding an exogenous stimulus, namely *bis-ns*-Q[10]. The supramolecular nature of intramolecular cross-linking within individual polymer chains in water, as revealed in this study, signifies a progression in the pursuit of creating synthetic materials with aqueous-phase behaviour similar to the self-folding exhibited by peptide macromolecules.

Recently, the Kim group used *bis-ns*-Q[10] and a four-armed polyethylene glycol (PEG) adamantane (AdA-4-arm-PEG) guest to construct a self-healable supramolecular hydrogel.[115] AdA-4-arm-PEG, which possesses two AdA molecules, can be specifically recognized by *bis-ns*-Q[10]. This recognition allows the two cavities of *bis-ns*-Q[10] to selectively encapsulate AdA molecules, forming ternary complexes through host–guest interactions during the hydrogel formation process. The dynamic and selective nature of this host–guest interaction enables the supramolecular hydrogel to rapidly restore its physical properties following damage, with these properties remaining largely unchanged even after multiple self-repair cycles. The approach to preparing self-healing supramolecular hydrogels offers insights into the design of soft materials with controllable physical properties and extended service life.

Bis-ns-Q[10] along with viologen-derived guests has also been used to prepare [5]rotaxane, linear supramolecular polymers, and supramolecular organic frameworks (Fig. 10).[116] Upon complexation of compound M1 (Fig. 10, bottom left), tetramethyl Q[6], and *bis-ns*-Q[10], a [5]rotaxane was formed. A supramolecular polymer with a molecular weight of 4.3×10^4 Da was produced when Q[7] and *bis-ns*-Q[10] interacted with the elongated compound M2. A three-dimensional supramolecular organic framework was formed through the self-assembly of *bis-ns*-Q[10] and the tetracationic tetrahedral monomer M3. It should be noted that a key role as cross-linkers in the formation of these supramolecular systems was played by *bis-ns*-Q[10].

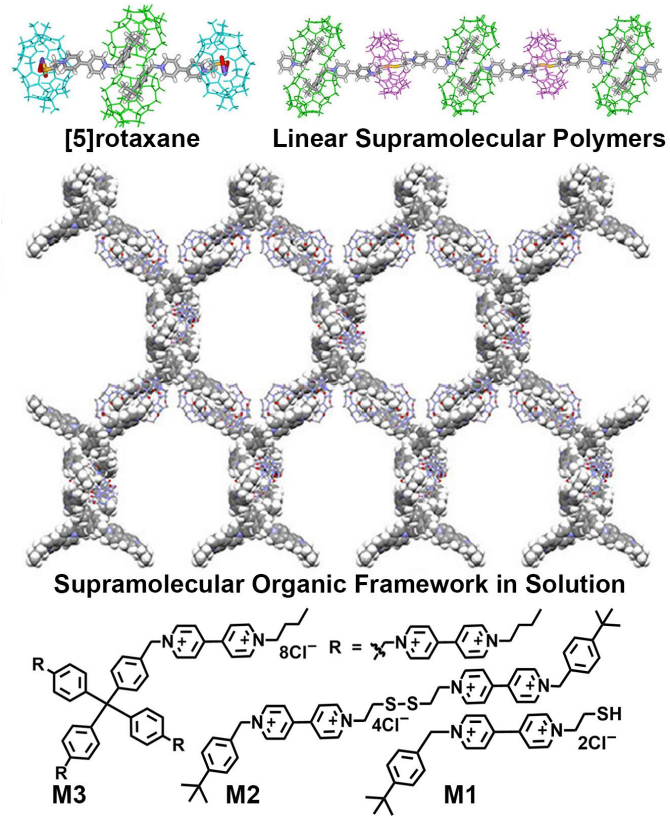

Fig. 10 Schematics of [5]rotaxane, linear supramolecular polymer, and 3D supramolecular framework model structures formed by *bis-ns*-Q[10] with M1, M2, and M3, respectively. Reproduced with permission from ref. 116. Copyright 2023, Elsevier Ltd.

4.2 Supramolecular polymers based on *t*Q[14]

Initially, our group explored supramolecular polymers of *t*Q[14] using 4,4'-bipyridine derivatives to interact with *t*Q[14]. Unfortunately, only shell-like 1:1 inclusion complexes were formed; the expected supramolecular polymers were not obtained.[108] Subsequently, our group successfully constructed the first supramolecular polymer of *t*Q[14] (*t*Q[14]-TBPyP) using the host–guest interaction between *t*Q[14] and 5,10,15,20-tetrakis (*N*-butyl-4-pyridinium) porphyrin tetrabromide (TBPyP).[50] TBPyP exhibits excellent water solubility, which enables supramolecular polymerization with the water-soluble *t*Q[14]. Gratifyingly, simply mixing *t*Q[14] and TBPyP in an aqueous solution afforded a supramolecular network, *t*Q[14]-TBPyP, driven by the host–guest interactions between the two molecules. Moreover, the addition of KCl effectively disassembled the *t*Q[14]-TBPyP assembly, liberating TBPyP (Fig. 11a). This shift occurred because the potassium ion readily coordinated with the carbonyl oxygen of the port of *t*Q[14], preventing TBPyP from complexing with *t*Q[14], thus dissociating the original assembly.

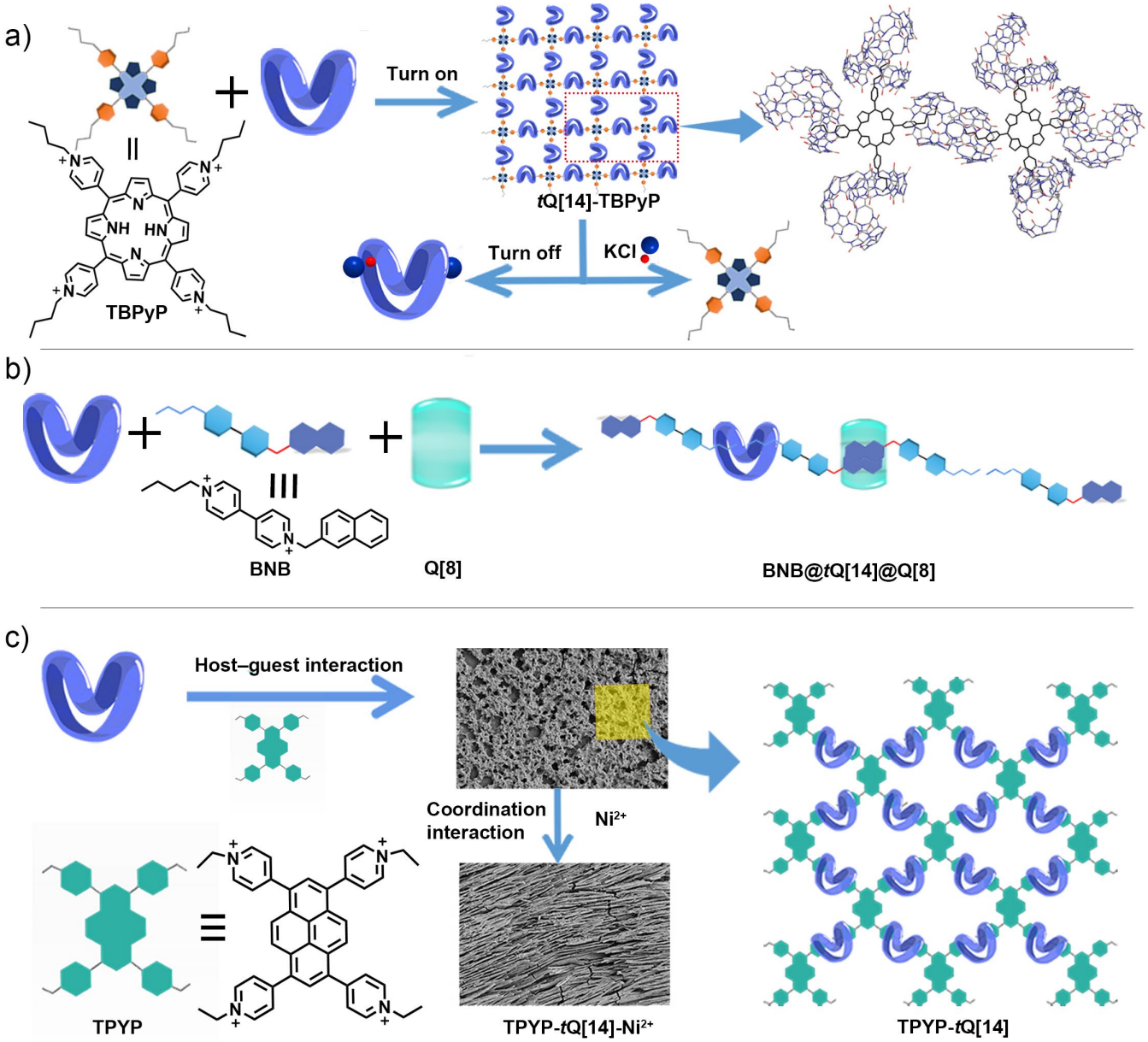

Fig. 11 a) Supramolecular polymer of *t*Q[14]-TBPyBp; b) Structures of *t*Q[14], BNB and Q[8] and illustration of supramolecular polymer; c) The structure of supramolecular polymers formed by *t*Q[14] and TPYP and morphological conversion of supramolecular polymers. Reproduced with permission from ref. 118. Copyright 2022, American Chemical Society.

After the successful synthesis of the supramolecular polymer of *t*Q[14], our group attempted to control the structure of the *t*Q[14]-based supramolecular polymers by introducing monomers bearing various functional groups. We fabricated *t*Q[14]-based linear supramolecular polymers with tuneable properties by an effective self-sorting strategy using *t*Q[14], Q[8], and 1-butyl-1'-(naphthalen-2-ylmethyl)-4,4'-bipyridinium bromide (BNB) (Fig. 11b).[117] The alkyl groups of BNB were inserted into the cavities of *t*Q[14], while the naphthyl part of BNB was encapsulated aided by π–π stacking in the Q[8] cavity, providing the driving force for supramolecular polymerization. Linear supramolecular polymers with controllable properties were obtained through the self-sorting of monomers BNB, *t*Q[14], and Q[8]. Such supramolecular polymers can be depolymerized by adding AH to the system. AH is a tight binder for Q[8], and outcompetes the two BNB guest molecules for the Q[8] cavity, thereby causing depolymerization.

As a further step to endow *t*Q[14] supramolecular polymers with useful functions, our group designed a water-soluble fluorescent tetrapyridinium pyrene compound (TPYP) to develop *t*Q[14]-based fluorescent materials. *t*Q[14], through host–guest interactions, bound to the alkyl chains and pyridinium of TPYP (*t*Q[14]:TPYP = 2:1) to form TPYP-*t*Q[14], a loose and porous supramolecular polymer (Fig. 11c).[118] Notably, the addition of Ni^{2+} to the TPYP-*t*Q[14] solution affected the morphology of the TPYP-*t*Q[14] and transformed it from a loose porous structure to a chain-like structure (Fig. 11c). The novelty of this structure stems from the unique structure of *t*Q[14], which has three metal-coordination sites and two unique cavities. These two cavities of *t*Q[14] bind to TPYP through host–guest interactions, while the third portal of *t*Q[14] (namely, Eu2 in Fig. 4a) coordinates with Ni^{2+}, forming a metal-mediated supramolecular polymer. These studies provide a new approach to control the structure of polymers through ligand-type interactions.

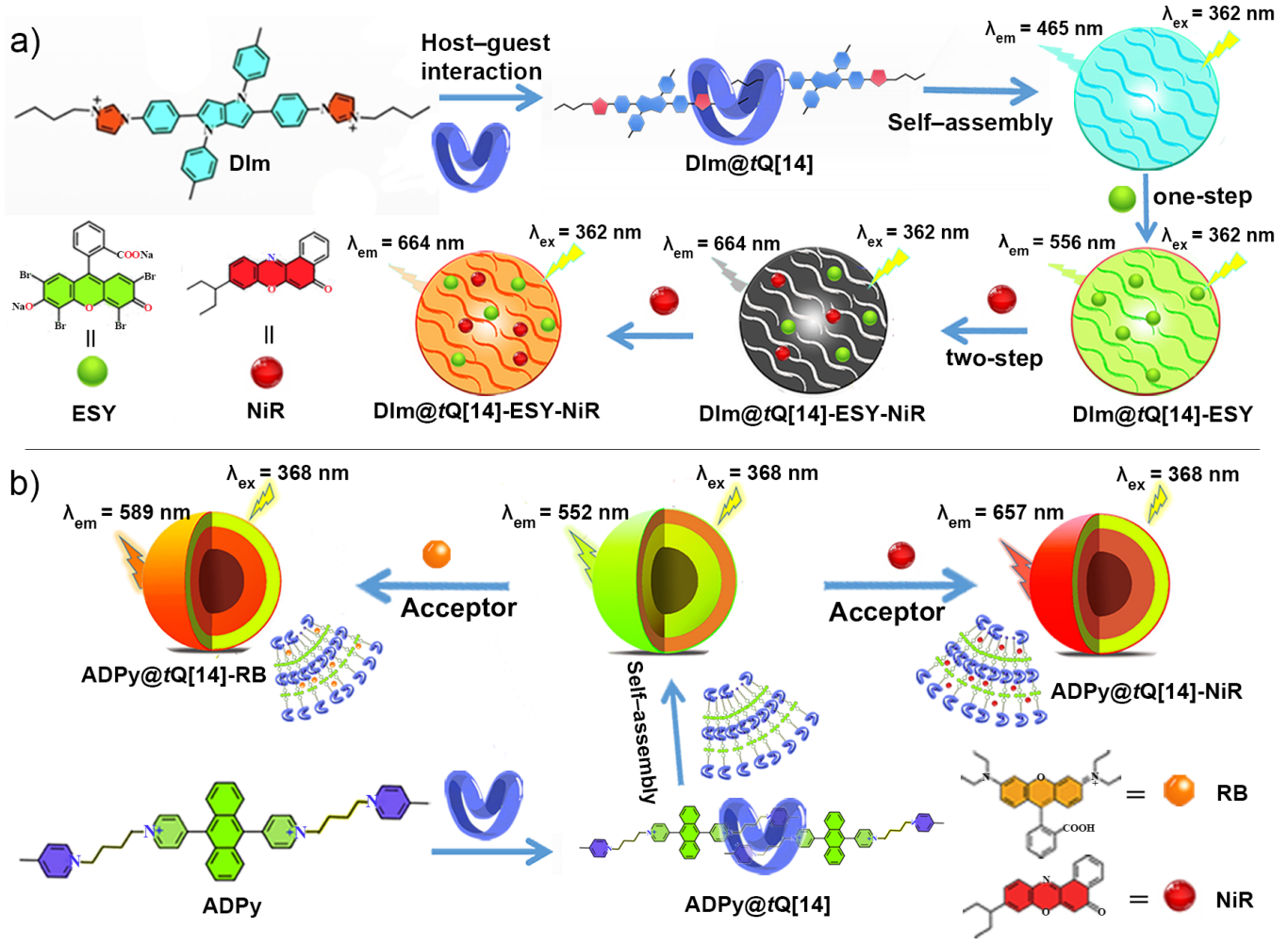

Fig. 12 a) Construction of linear supramolecular polymers (DIm@*t*Q[14]) and DIm@*t*Q[14]-based aqueous ALSHs. Reproduced with permission from ref. 119. Copyright 2022, Elsevier Ltd; b) Spherical supramolecular polymers (ADPy@*t*Q[14]) for application as ALHSs.

Inspired by the luminescence behaviour of the fluorescent supramolecular polymer material constructed by *t*Q[14], our group synthesized a linear supramolecular polymer, DIm@*t*Q[14] (n_{DIm}:$n_{tQ[14]}$ = 1:1), using imidazole derivatives (DIm) and *t*Q[14] via host–guest interactions in aqueous solution (Fig. 12a).[119] DIm and *t*Q[14] formed staggered and overlapping linear supramolecular polymers (n_{DIm}:$n_{tQ[14]}$ = 1:1 and average particle size = 214 nm) with intense fluorescence achieved through self-assembly. This intense fluorescence was attributed to the formation of supramolecular polymers (DIm@*t*Q[14]) via self-assembly and interaction of the alkyl chains and imidazole groups of DIm with the cavities of *t*Q[14]. Planar stacking restricted the intramolecular rotation of the DIm, resulting in a less easy dissipation of the molecular excited state energy, which ultimately led to significant aggregation-induced emission (AIE) effects. The favourable AIE effect of the supramolecular polymer DIm@*t*Q[14] means that it can serve as an excellent donor for the construction of artificial light-harvesting systems (ALHSs) in aqueous solution. Eosin Y (ESY), whose absorption wavelength adequately overlaps with the emission band of DIm@*t*Q[14] and thereby generates new emission bands, was selected as the receptor to construct an ALHS in an aqueous solution together with DIm@*t*Q[14]. ESY is easily trapped randomly by noncovalent interactions in the staggered crossing and overlapping linear structure of DIm@*t*Q[14]. Finally, DIm@*t*Q[14] was successfully used to construct an ALHS in water by loading ESY ($n_{DIm@tQ[14]}$:n_{ESY} = 200:1) with a one-step energy-transfer efficiency of 42.67%. In nature, processes such as photosynthesis typically involve continuous, multi-step energy transfers. Inspired by this natural phenomenon, a two-step energy-transfer light-harvesting system was conceptualized. This system used DIm@*t*Q[14]-ESY as the donor and Nile Red (NiR) as the acceptor, and the absorption band of NiR closely aligned with the fluorescence emission of the DIm@*t*Q[14]-ESY assembly. Impressively, an efficient system boasting an energy-transfer efficiency of 91.47% was achieved for the two-step energy-transfer setup when DIm@*t*Q[14]/ESY/NiR was at a ratio of 200/1/2. Moreover, a rudimentary white-light-emitting diode (LED) was developed by simply applying a concentrated solution of the DIm@*t*Q[14]-ESY-NiR assembly (200:1:1) to the surface of a commercial 365 nm ultraviolet (UV) LED. When the LED was switched on, the diode without the DIm@*t*Q[14]-ESY-NiR coating emitted only weak light. In contrast, the LED coated with DIm@*t*Q[14]-ESY-NiR (200:1:1) emitted white light, demonstrating its potential applicability in white-light-emitting materials.

Similarly, our group designed two efficient ALHSs (ADPy@*t*Q[14]-NiR and ADPy@*t*Q[14]-RB) by the supramolecular self-assembly of anthracene derivatives (ADPy), *t*Q[14], NiR, and Rhodamine B (RB) in the aqueous phase (Fig. 12b).[120] The two butyl chains of ADPy with terminal pyridinium moieties can form stable inclusion complexes with *t*Q[14] and self-assemble into spherical supramolecular polymer ADPy@*t*Q[14] ($n_{tQ[14]}$:n_{ADPy} = 1:1 and average particle size = 327.24 nm). The ALHSs (ADPy@*t*Q[14]-NiR and ADPy@*t*Q[14]-RB) constructed by our group using ADPy@*t*Q[14] as a donor and NiR and RB as acceptors have the advantages of a long fluorescence lifetime, a high fluorescence quantum yield, and an antenna effect. In particular, the ADPy@*t*Q[14]-NiR assembly shows a remarkable antenna effect (52.4) and a high energy-transfer efficiency of 72.45%, similar to that exhibited by natural illumination systems.

Chemical Society Review

REVIEW

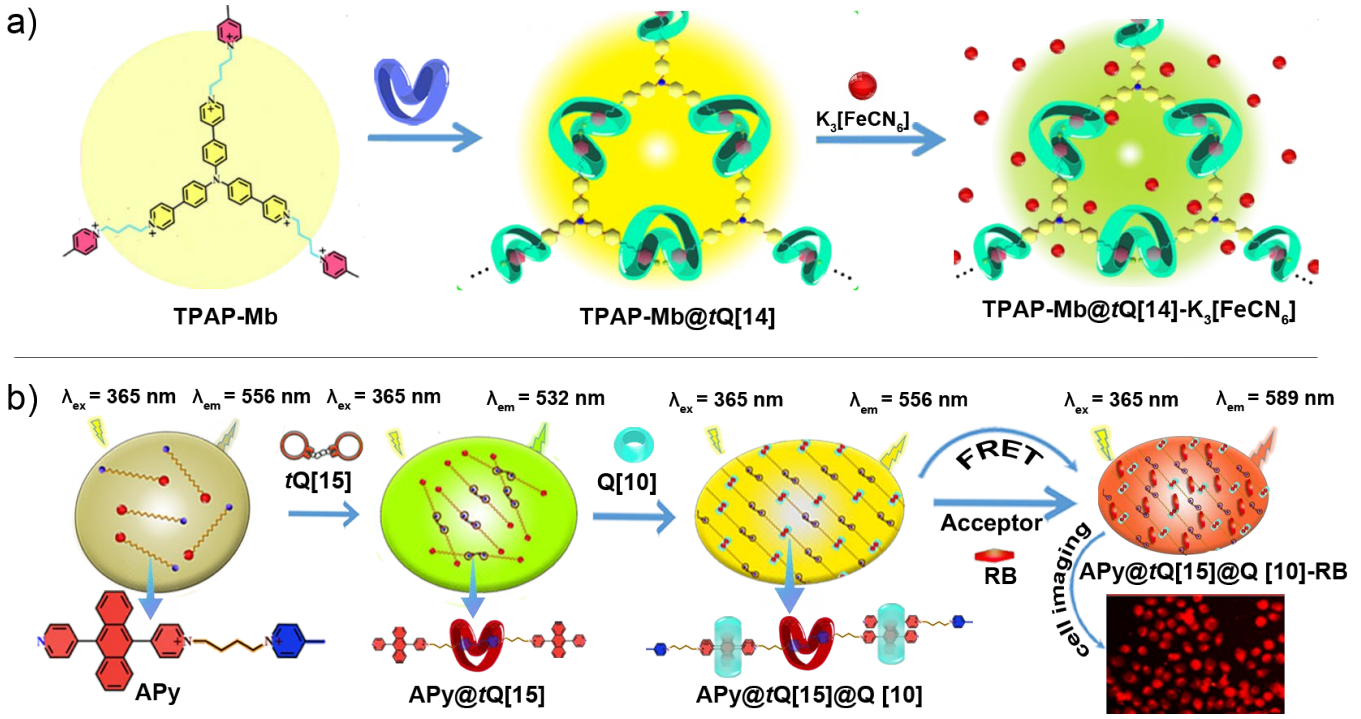

Fig. 13 a) Schematic of the construction of AIE supramolecular polymers and the removal of anions. Reproduced with permission from ref. 106. Copyright 2022, American Chemical Society; b) Schematic of self-assembled APy@*t*Q[15]@Q[10]-based aqueous light-harvesting system. Reproduced with permission from ref. 121. Copyright 2022, Elsevier Ltd.

Recently, our group prepared a net-like AIE supramolecular polymeric material (TPAP-Mb@*t*Q[14]) through supramolecular self-assembly of *t*Q[14] and a triphenylamine derivative (TPAP-Mb) (Fig. 13a).[106] Based on the AIE molecule triphenylamine, a TPAP-Mb guest molecule tailored for *t*Q[14] was designed. The alkyl chain segment and the methylpyridine fraction of TPAP-Mb can interact with *t*Q[14] through host–guest interactions, thus limiting the intramolecular rotational effect of TPAP-Mb and affording an AIE fluorescent supramolecular polymer, TPAP-Mb@*t*Q[14] ($n_{\text{TPAP-Mb}}$:$n_{t\text{Q[14]}}$ = 2:3 and particle size = 280–410 nm). Notably, among the different types of anions (F^-, Cl^-, Br^-, I^-, HIO^{3-}, SCN^-, $Fe(CN)_6^{3-}$, SO_4^{2-}, $H_2PO_4^-$, $P_2O_7^{4-}$, $S_2O_3^-$, ClO_4^-, AC^-, NO_3^-, and CO_3^{2-}) that were added to the aqueous solution of TPAP-Mb@*t*Q[14], only $Fe(CN)_6^{3-}$ led to a sharp decrease in the fluorescence intensity of TPAP-Mb@*t*Q[14]. The fluorescence colour changed from bright yellow to dark. These phenomena indicate the high selectivity of TPAP-Mb@*t*Q[14] for $Fe(CN)_6^{3-}$. This specific quenching effect may be due to the competitive absorption mechanism between $Fe(CN)_6^{3-}$ and TPAP-Mb@*t*Q[14]. Specifically, the emission spectrum of TPAP-Mb@*t*Q[14] exhibits overlaps with the absorption spectrum of $Fe(CN)_6^{3-}$, while there is minimal overlap with that of the other anions. The effective absorption of $Fe(CN)_6^{3-}$ impedes the excitation of TPAP-Mb@*t*Q[14]. Subsequently, fluorescence titration experiments were conducted to determine the limit of detection of TPAP-Mb@*t*Q[14] for $Fe(CN)_6^{3-}$ as 1.64×10^{-7} M. Interestingly, TPAP-Mb@*t*Q[14] was also effective in removing residual $Fe(CN)_6^{3-}$ from aqueous solutions (removal efficiency 97.38%). When $Fe(CN)_6^{3-}$ was gradually added to the TPAP-Mb@*t*Q[14] solution, the charge of the system is redistributed because of electrostatic interactions, forcing the colloidal particles to aggregate into larger particles and precipitate, resulting in the purification and removal of $Fe(CN)_6^{3-}$ from water. In addition, *t*Q[14] could be recovered from a mixed solution of acetone/chloroform ($V_{\text{acetone}}/V_{\text{chloroform}}$ = 1:1) via elution by high-speed centrifugation with a recovery of 68.3%. This work offers a prospective application of AIE supramolecular polymeric

materials containing *t*Q[14] for addressing environmental water pollution issues.

4.3 Supramolecular polymers based on *t*Q[15]

The abovementioned discussion has demonstrated that the supramolecular polymer of *t*Q[14] can be used to construct ALHSs. Therefore, after successfully obtaining the ALHSs of *t*Q[14], our group decided to construct an ALHS comprising *t*Q[15] supramolecular polymers (Fig. 13b).[121] Firstly, the 4-picolinium group of the anthracene derivative (APy) was encapsulated by *t*Q[15] through a host–guest interaction to form the supramolecular monomer APy@*t*Q[15] (n_{APy}:$n_{tQ[15]}$ = 2:1). The introduction of Q[10] facilitated the formation of the supramolecular polymer APy@*t*Q[15]@Q[10] through π–π interactions between the anthracene groups of distinct APy molecules within the Q[10] cavity. Scanning electron microscopy and transmission electron microscopy results showed that APy@*t*Q[15]@Q[10] has a staggered chain configuration, which implies that the supramolecular polymer was formed via a chain-growth mechanism. Dynamic light scattering revealed an increase in the average particle dimension from 50.4 nm (APy) to 152.3 nm (APy@*t*Q[15]@Q[10]). APy@*t*Q[15]@Q[10] is a supramolecular polymer with AIE characteristics. It can be used to circumvent the conventional aggregation-induced quenching. Hence, APy@*t*Q[15]@Q[10] could be employed as a donor for establishing an ALHS in water. Therefore, ALHS (APy@*t*Q[15]@Q[10]-RB) was successfully constructed in an aqueous medium using APy@*t*Q[15]@Q[10] as a donor and RB, whose absorption band greatly overlapped with the emission band of APy@*t*Q[15]@Q[10], as an acceptor. The APy@*t*Q[15]@Q[10]-RB ($n_{APy@tQ[15]@Q[10]}$:n_{RB} = 200:1) system exhibited a remarkable antenna effect (17.65) and a substantial energy-transfer efficiency (41.37%). Hence, it can be used as a promising novel multicolour cell-labeling imaging agent. Cellular experiments showed the efficient entry of APy@*t*Q[15]@Q[10] and APy@*t*Q[15]@Q[10]-RB into HeLa cells via endocytosis, with their subsequent accumulation in the cell nucleus. Hence, these systems can be employed for nuclear labeling and live-cell tracking applications. APy@*t*Q[15]@Q[10]-RB can also characterize cell morphology. The efficient ALHSs generated in this study using a supramolecular assembly strategy show great promise for labeling and tracking live cells, thereby broadening the application scope of the Q[*n*] system in the field of biology.

4.4 Supramolecular polymers based on dimeric Q[6]

The Isaacs group explored the ability of Q[6]–Q[6]2 to undergo supramolecular polymerization when bonded with PEG-derived divalent guests PEG-R_{MW} (PEG-R_{300}, PEG-R_{1000}, PEG-R_{3350}, and PEG-R_{10000}; molecular weight (MW) = 300, 1000, 3350, and 10000, respectively) with different molecular weights (Fig. 14).[122] When Q[6]–Q[6]2 is combined with the longest PEG-derived guest PEG-R_{10000} (MW = 10000) by self-assembly, supramolecular polymers (PEG-R_{10000})$_n$@(Q[6]–Q[6]2)$_n$ with an oligomerization degree of at least 36 can be formed, whereas PEG-R_{300}, PEG-R_{1000}, and PEG-R_{3350} formed only (cyclic) oligomers with low polymerization degree. This is mainly because the short and flexible PEG chains of the shorter PEG-derived guest (PEG-R_{300}, PEG-R_{1000}, and PEG-R_{3350}) can adjust their conformation to facilitate the formation of small (cyclic) oligomers. In contrast, PEG-R_{10000} can form supramolecular polymers because of the entropic costs associated with the conformational restriction of PEG-R_{10000} with long PEG chains. Interestingly, the degree of polymerization of such supramolecular polymers decreased from 36-mer to 22-mer after 14 days, which can be attributed to the continuous slow dissociation of the hexanediammonium (HDA) moiety of PEG-R_{10000} from the Q[6]-sized cavity of Q[6]–Q[6]2. This observation underscores the possibility of dynamic changes in Q[*n*]-derived supramolecular systems owing to the typically sluggish kinetics of association and dissociation between Q[*n*] and guest molecules.

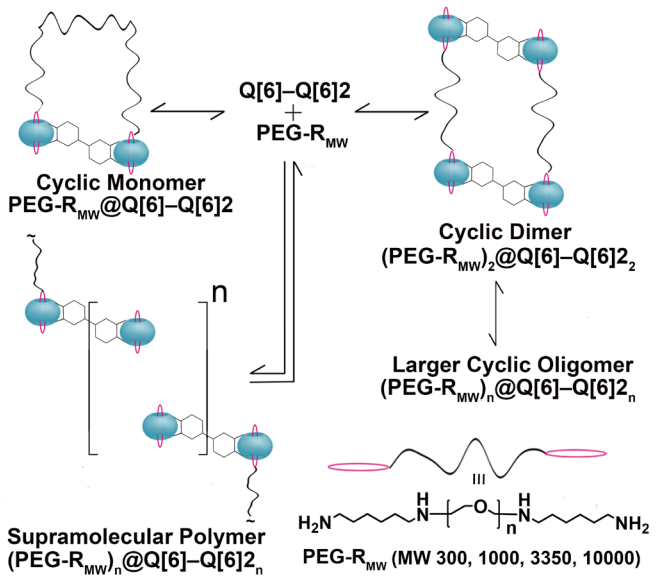

Fig. 14 Divalent guests derived from PEG derivatives with different molecular weights and schematic of the formation of supramolecular polymers.

5. Oligomers

An oligomer is a molecule consisting of several repeating units and is a concept that relates to that of a polymer (polymers usually have thousands or millions of units). The units of an oligomer may be connected by covalent bonds or weaker forces, such as hydrogen bonds. When a guest molecule engages with double-cavity Q[*n*]s, it results in the formation of not only supramolecular polymers but also oligomers for

diverse reasons. These oligomers can manifest intriguing properties and atypical effects.

5.1 Oligomers based on *bis-ns*-Q[10]

While attempting to prepare a supramolecular polymer of *bis-ns*-Q[10], the Isaacs group also designed a collection of guest molecules featuring dual adamantylammonium (Ad) groups, spaced apart by xylylene linkers. However, because of dimerization and cyclization that occur when these guests interact with *bis-ns*-Q[10], only oligomers with molar ratios of 1:1 or 2:2 are eventually formed. Considering the effect of chain length, the Isaacs group replaced xylylene with biphenyl, which also resulted in oligomers with a molar ratio of only 2:2. Hence, they suggested that no supramolecular polymer could form because of the presence of dual identical Ad-binding domains. Therefore, they designed the guest molecule Ad-PXDA-HDA containing Ad, HDA, and *p*-xylylenediamine (PXDA)-binding domains (Fig. 15a).[105] When

Fig. 15 a) Manipulation of complex stoichiometry and extension by reversible chemical stimuli; b) Possible pathways of [3]rotaxane formation.

$n_{bis\text{-}ns\text{-}Q[10]}$:$n_{Ad\text{-}PXDA\text{-}HDA}$ = 1:1, the Ad-PXDA-HDA was forced to use both Ad- and HDA-binding domains to fill both cavities of *bis-ns*-Q[10], thereby forming (Ad-PXDA-HDA)$_2$@*bis-ns*-Q[10]$_2$. When $n_{bis\text{-}ns\text{-}Q[10]}$:$n_{Ad\text{-}PXDA\text{-}HDA}$ = 1:2, Ad-, PXDA-, and HDA-binding domains enter each cavity of *bis-ns*-Q[10] to form (Ad-PXDA-HDA)$_2$@*bis-ns*-Q[10] with three isomers. Moreover, this change can be reversibly transformed by regulating the host–guest molar ratio. Next, they attempted to determine whether Q[6] and Q[7] can act as external chemical stimuli to control the molecular weight of *bis-ns*-Q[10] when interacting with Ad-PXDA-HAD. The results showed that because of the high K_a value of Q[6] with the HDA-binding domain, the addition of Q[6] caused its selective complexation to the HDA-binding domain, which spatially limited binding to the PXDA-binding domain of Ad-PXDA-HDA, leaving only the Ad-binding domain to complex with *bis-ns*-Q[10], thereby forming (Ad-PXDA-HDA)$_2$@*bis-ns*-Q[10]$_2$@Q[6]$_2$. Surprisingly, (Ad-PXDA-HDA)$_2$@*bis-ns*-Q[10]$_2$@Q[6]$_2$ is longer than the precursor mixture of the diastereoisomers of (Ad-PXDA-HDA)$_2$@*bis-ns*-Q[10] on average. Finally, the extremely high binding affinity of Q[7] for the adamantine ion was utilized to control the contraction of (Ad-PXDA-HDA)$_2$@*bis-ns*-Q[10]$_2$@Q[6]$_2$ to form Ad-PXDA-HDA@Q[7]@Q[6]. Reversible control of the stretching of such supramolecular systems can be used for forming stimulus-responsive molecular machines (*e.g.*, molecular muscles).

The Isaacs group synthesized [3]rotaxane G$_2$@IM-*bis-ns*-Q[10] (Fig. 15b) in 69% yield by stirring a mixture of *bis-ns*-CB[10], 1,6-hexanediamine derivative (G), formaldehyde, and imidazolidone at 50 °C under acidic conditions (8 M HCl) for 1 h.[90] Furthermore, experimental results confirmed that G$_2$@IM-*bis-ns*-Q[10] was a [3]rotaxane. For example, treatment of G$_2$@IM-*bis-ns*-Q[10] with 0.1 M of sodium hydroxide in methanol did not cause its dissociation; Stirring G$_2$@IM-*bis-ns*-Q[10] with *p*-phenylenediamine (10 equiv.) or 1,6-hexanediamine dihydrochloride (10 equiv.) in D$_2$O at 50 °C did not cause any guest exchange. Fig. 15b shows two possible pathways (slippage and clipping) for the formation of G$_2$@IM-*bis-ns*-Q[10]. Three experiments were conducted to show that the clipping pathway was the main way to form G$_2$@IM-*bis-ns*-Q[10]. Firstly, G$_2$@*bis-ns*-Q[10], imidazolidone, and formaldehyde reacted rapidly to produce G$_2$@IM-*bis-ns*-Q[10]. Secondly, a mixture of G$_2$@IM-*bis-ns*-Q[10] and 1,6-hexanediamine dihydrochloride was heated, which, however, did not produce (1,6-hexanediamine dihydrochloride)$_2$@IM-*bis-ns*-Q[10]. Hence, G does not undergo a slippage process with IM-*bis-ns*-Q[10]. Finally, heating IM-*bis-ns*-Q[10] and G mixed in D$_2$O (50 °C) did not yield G$_2$@IM-*bis-ns*-Q[10]. This method of clipping Q[*n*]-type macrocycles onto preformed shafts or rings is expected to afford more complex molecular machines based on Q[*n*]s compared to those prepared by other methods.

5.2 Oligomers based on *t*Q[14]

Our group investigated the *t*Q[14]-ThT host–guest system constructed from *t*Q[14] and thioflavin T (ThT), which can recognize alkaline earth metal ions and form solid photoluminescent complexes.[101] Since *t*Q[14] has two side cavities, it can contain a methylated benzothiazole of one ThT and a dimethylaminobenzene unit of another ThT (Fig. 16a), which may lead to the formation of different supramolecular oligomers in the interacting system of *t*Q[14]-ThT (Fig. 16b and c). The structure of *t*Q[14] with two side cavities and the ability of *t*Q[14] to form oligomers with ThT impart recognition properties to *t*Q[14]. In this system, the section of ThT not encapsulated in the *t*Q[14] cavity is surrounded by excess *t*Q[14] molecules interacting through their outer surfaces (Fig. 16c), dramatically enhancing the fluorescence intensity even at very high *t*Q[14]/ThT ratios.

Fig. 16 Possible interaction modes of *t*Q[14] and ThT.

5.3 Oligomers based on dimeric Q[6]

The Isaacs group used the double-cavity Q[6]–Q[6]1 host along with a series of guests containing HDA units and viologen

units to create a range of supramolecular ladders with two and three rungs (Fig. 17).[92] Since each cavity of Q[6]–Q[6]1 retains the binding capacity of Q[6] itself, the HDA unit constitutes a strong binding site for each cavity of Q[6]–Q[6]1. Although the larger viologen moiety has a weaker binding affinity for Q[6]-sized cavities, it does not prevent it from shuttling through each cavity. Using this methodology, two- and three-rung ladders were successfully achieved. However, the analogous four-rung ladder was not obtained, perhaps because of the competition between the formation of the related looped structure and the assembly of the four-rung supramolecular ladder. Impressively, the three-rung supramolecular ladder (nanoscale dimensions: 2.6 × 4.0 nm and relative molecular mass: 7389) was within the range of small proteins. This work provides further evidence that the synthesis of double-cavity Q[*n*] compounds can produce highly complex Q[*n*] structures. In addition, the availability of Q[6] dimers, coupled with the prospects for constructing advanced multivalent Q[*n*] scaffolds, may broaden the range of binding epitopes. These binding epitopes can induce the dimerization and formation of more complex assemblies of appropriate nanoscale objects such as proteins, polymers, and nanoparticles.

Fig. 17 Formation of supramolecular ladders from Q[6]–Q[6]1 and oligomeric viologen derivatives.

Oligomers derived from double-cavity Q[*n*]s possess lower molecular weights than the corresponding supramolecular polymers of double-cavity Q[*n*]s. Nevertheless, they play a crucial role in the fabrication of molecular machines, such as molecular muscles. With the design of specialized guest molecules and the utilization of suitable preparation techniques, the creation of more intricate molecular machines is anticipated.

6. Sensors

In recent years, the study and fabrication of organic fluorescence sensors have aroused great interest because they exhibit high luminescence efficiency and good selectivity.[123–126] This has led to the rapid development of the field of supramolecular fluorescent probes constructed using host–guest complexes.[127–129] Double-cavity Q[*n*]s constitute an excellent platform for designing supramolecular chemical sensors because of the confluence of desirable properties, including chemical inertness, non-toxicity to organisms, high affinity for various organic analytes in water, and rapid host–guest binding kinetics. Detection methods using host–guest indicator complexes by employing double-cavity Q[*n*]s as optical sensors have already been applied in biological cells, wastewater, and drinking water. They have also been used to detect cations, anions, and neutral molecules.[101,102,130,131] Such methods can be translated for use in *in vivo* and *in vitro* sensing and imaging systems. Thus, double-cavity Q[*n*]s can be highly useful in the fields of sensing and imaging.

6.1 Sensors based on *bis-ns*-Q[10]

Our group explored molecular recognition triggered through the host–guest interaction of *bis-ns*-Q[10] and pyrene-adamantaneammonium (*P*-ADA) guests (Fig. 18a).[130] As described above, three diastereomers (top–top, center–center, and top–center) are possible when *bis-ns*-Q[10] interacts with asymmetric guests such as *P*-ADA. The monomer and excimer fluorescence emissions of pyrene imposed by the aforementioned three different diastereomers within the ternary complex with *bis-ns*-Q[10] were expected to be different. The experimental results indicated that the different photophysical signals of pyrene from these three possible diastereomers can be used to identify the top–center isomer of the ternary complexes of ADA derivatives with the hosts. As shown in Fig. 18b, in aqueous solution (pH = 2), the free-state *P*-ADA produces typical monomeric emission near 378 and 396 nm when excited at 340 nm. Similarly, the maximum emission intensity near 485 nm (typical excimer emission of pyrene) increases when increasing concentrations of *bis-ns*-Q[10] are added to the *P*-ADA solution. The spectrum of *P*-ADA exhibits the excimer emission bands because in the ternary complexes with the top–center configuration, the two identical cavities of *bis-ns*-Q[10] lead to intermolecular π–π stacking interactions between the two pyrene units of *P*-ADA, resulting in the excimer emission band of *P*-ADA. Thus, the top–center isomer of the *P*-ADA@*bis-ns*-Q[10] ternary complex can be easily determined by the optical signal of the change in the monomer/excimer fluorescence emissions of the pyrene groups on *P*-ADA. In addition, the imidazolidone derivative of *bis-ns*-Q[10] (IM-*bis-ns*-Q[10]) shows similar binding interactions with *P*-ADA.

Fig. 18 a) Formation of three diastereomers when *P*-ADA binds to *bis-ns*-Q[10]; b) Changes in fluorescence spectra of *P*-ADA (10.0 μM) aqueous solution (298 K, pH = 2.0) after the addition of different concentrations of *bis-ns*-Q[10]. Reproduced under the terms of the CC–BY Creative Commons Attribution 4.0 International License (https://creativecommons.org/licenses/by/4.0/).

Recently, our group constructed a supramolecular fluorescent probe (APFG@*bis-ns*-Q[10]), which is specific and sensitive to ClO^-, through a noncovalent host–guest interaction between *bis-ns*-Q[10] and positively charged Astrazon Pink FG (APFG).[131] Given the good match of the double cavity of *bis-ns*-Q[10] with the *N*-(2-chloroethyl)-*N*-methylaniline moiety of the APFG guest, the rotation of this unit is restrained and the intramolecular charge-transfer effect leads to orange-red fluorescence of the APFG@*bis-ns*-Q[10] probe. The interaction

of APFG@*bis*-*ns*-Q[10] with ClO^- oxidizes the C–C double bond in APFG, leading to the cleavage of the APFG molecule and eventually causing the fluorescence quenching of the APFG@*bis*-*ns*-Q[10] probe (Fig. 19a). The experimental results showed that APFG@*bis*-*ns*-Q[10] can specifically detect ClO^- without interference by 20 different anions (HPO_4^{2-}, HSO_3^-, I^-, Br^-, CO_3^{2-}, HSO_4^-, PO_4^{3-}, SO_3^{2-}, NO_3^-, SCN^-, SO_4^{2-}, IO_3^-, CH_3COO^-, $H_2PO_4^{2-}$, SiO_4^{2-}, HCO_3^{2-}, S^{2-}, OH^-, Cl^-, and NO_2^-). In addition, APFG@*bis*-*ns*-Q[10] has good optical properties, excellent biocompatibility, and low toxicity. Consequently, APFG@*bis*-*ns*-Q[10] was successfully used for imaging HK2 and HeLa cells (Fig. 19b). This study demonstrates the potential application of *bis*-*ns*-Q[10] for probing studies and cellular imaging can be highly useful for studies on probes and for imaging in cells.

Fig. 19 a) Construction of supramolecular complex APFG@*bis*-*ns*-Q[10] and its mechanism for detecting ClO^-; b) Fluorescence photographs (365 nm UV lamp) of APFG and APFG@*bis*-*ns*-Q[10] in aqueous solution, and their application in cellular imaging for the detection of ClO^-. Reproduced with permission from ref. 131. Copyright 2023, Elsevier Ltd.

6.2 Sensors based on *t*Q[14]

Given the importance of amino acids for life, our group also investigated the interaction between *t*Q[14] and 20 amino acids in an acidic aqueous solution and DMSO.[103] We found that *t*Q[14] demonstrates a poor binding affinity for amino acids with hydrophobic or polar side chains. In contrast, *t*Q[14] exhibits a significantly high binding affinity for amino acids with positively charged side chains or aromatic rings.

*t*Q[14] shows good solubility in both neutral water and DMSO and an atypical binding behaviour towards guest molecules and metal ions, thereby providing a route to fabricate host–guest supramolecular fluorescent sensors. Indeed, our group succeeded in obtaining a water-soluble fluorescent sensor consisting of *t*Q[14] and thiazole orange (TO) complexes with distinct fluorescence responses to Hg^{2+}, Ba^{2+}, and Pb^{2+}.[102] *t*Q[14] selectively binds to the benzothiazole moiety of TO in aqueous solution and restricts the rotation of the individual C–C bonds of TO, forming a stable *t*Q[14]/TO complex that fluoresces more strongly than free TO. Absorption and fluorescence spectra indicate that the *t*Q[14] molecule interacts with not only the TO monomer but also the TO dimer. The twisted conformation of *t*Q[14] results in a more concentrated distribution of carbonyl oxygen atoms at its ports, implying a strong affinity for metal ions. Based on this, we employed fluorescence spectroscopy to study the influence of metal ions on the fluorescence of the *t*Q[14]/TO system. When Hg^{2+} (<60 μM) was added into the *t*Q[14]/TO (2:1) system, the fluorescence of TO was initially enhanced. However, a further increase in the concentration of Hg^{2+} (>100 μM) resulted in fluorescence quenching. This phenomenon occurred because the initial addition of Hg^{2+} formed the ternary complex *t*Q[14]/TO/Hg^{2+} (Hg^{2+} < 25 equiv. of TO). The addition of more Hg^{2+} led to the creation of *t*Q[14]/Hg^{2+} and TO/Hg^{2+} complexes exhibiting minimal or undetectable fluorescence (Fig. 20a). The detection limit of *t*Q[14]/TO for Hg^{2+} was 7.8×10^{-8} mol/L. When Ba^{2+} was introduced into the *t*Q[14]/TO (2:1 and 15:1) systems, the fluorescence of TO was quenched. This behaviour might be attributed to the ability of Ba^{2+} to establish a coordination complex with *t*Q[14], triggering the release of TO molecules and resulting in fluorescence quenching (Fig. 20b and c). Notably, the *t*Q[14]/TO sensor can be reused to detect Ba^{2+} by adding SO_4^{2-} and the detection limit for Ba^{2+} was determined to be 3.2×10^{-6} mol/L. Under comparable conditions, the interaction of Pb^{2+} with *t*Q[14]/TO (15:1) led to partial fluorescence quenching because of the formation of the ternary complex *t*Q[14]/TO/Pb^{2+} (Fig. 20d). In addition, common metal ions (Cu^{2+}, Fe^{2+}, Fe^{3+}, Na^+, Co^{2+}, Cd^{2+}, Ca^{2+}, Al^{3+}, Zn^{2+}, Mn^{2+}, Ni^{2+}, Sr^{2+}, K^+, Li^+, Mg^{2+}, Cr^{3+}, Hg^{2+}, Ba^{2+}, and Pb^{2+}) in the environment do not interfere with the detection of the three abovementioned ions using the *t*Q[14]/TO system. This result shows that the *t*Q[14]/TO system exhibits remarkable selectivity in the qualitative detection of Hg^{2+}, Ba^{2+}, and Pb^{2+}. Therefore, it is highly desirable to develop a novel chromogenic chemosensor for Hg^{2+}, Ba^{2+}, and Pb^{2+} based on the *t*Q[14]/TO system.

Fig. 20 Possible detection mechanisms of the probe a) *t*Q[14]/TO (2:1) for Hg^{2+}; b) *t*Q[14]/TO (2:1) for Ba^{2+}; c) *t*Q[14]/TO (15:1) for Ba^{2+}; and d) *t*Q[14]/TO (2:1) for Pb^{2+}.

Using the abovementioned strategy of combining *t*Q[14] with fluorescent materials, our group reported alkaline earth metal ion-mediated solid photoluminescent complexes comprising thioflavin T (ThT) and *t*Q[14].[101] The *t*Q[14-ThT host–guest interaction system was first constructed (Fig. 16c), and was found to exhibit a specific response to alkaline earth metal ions. When the molar ratio of *t*Q[14] to ThT was 1:1, introducing Ca^{2+}, Sr^{2+}, or Ba^{2+} into the *t*Q[14]-ThT system caused fluorescence quenching. Conversely, the addition of Mg^{2+} enhances the fluorescence, which is then subsequently quenched. At a *t*Q[14]:ThT ratio of 1:15, introducing Mg^{2+}, Ca^{2+}, or Ba^{2+} produces ternary solid precipitates that exhibit vibrant blue fluorescence. However, the addition of Sr^{2+} quenched the fluorescence of the *t*Q[14]-ThT system. The *t*Q[14]-ThT

interaction system holds the potential for detecting alkaline earth metal ions and developing supramolecular photoluminescent materials that exhibit stimuli-responsive characteristics.

In addition to the fact that *t*Q[14] together with fluorescent compounds can constitute a probe, we have recently discovered that *t*Q[14] alone can also be used as a probe.[132] We found that *t*Q[14] exhibits fluorescence at elevated concentrations due to the cluster-triggered emission effect. So we tried to directly use *t*Q[14] as a probe for the detection of some metal ions. To test its broad sensing capabilities, selected transition metal ions (0.1 mM) were introduced into a formic acid solution with *t*Q[14] (Fig. 21a). The data underscored that only the addition of Fe^{3+} diminished the fluorescence intensity of *t*Q[14]. The quenching efficiency reached an impressive 95.47% at a Fe^{3+} concentration of 6 times the concentration of *t*Q[14] (Fig. 21b), confirming *t*Q[14]'s marked selectivity for Fe^{3+}. Fluorescence titration of *t*Q[14] and Fe^{3+} (Fig. 21c) further demonstrated the high precision of this method. *t*Q[14] exhibits a low detection limit for Fe^{3+} (1.71×10^{-5} M) and maintains a good linear fit, with minimal disturbance from other metal ions. This work positioned *t*Q[14] as an innovative fluorescent probe, and provides new ideas for the application of Q[*n*]s.

Fig. 21 a) Photographs of formic acid solutions of transition metal ions and *t*Q[14] under 365 nm UV-lamp irradiation; b) Fluorescence spectra of *t*Q[14] (0.5 mM) toward 6 equiv. of different M^{n+} (3.0 mM); c) Fluorescence titration for the detection of Fe^{3+} by *t*Q[14]. Reproduced with permission from ref. 132. Copyright 2022, Elsevier Ltd.

*t*Q[14] has size-selective cavities and O-donating sites, that is, it may exhibit luminescent responses to stimulation by organic guest species in polar solvents. Our group recognized that *t*Q[14] or *t*Q[14]–guest systems could be directly used to prepare probes for the detection of metal ions. Therefore, we extended this strategy to non-metallic cations and anions as well as to neutral molecules. We found that *t*Q[14] and two hemicyanine dyes (2-(4-(dimethylamino)styryl)-1-methylpyridinium iodide (2-ASP) and *trans*-4-[4-(dimethylamino)styryl]-1-methylpyridinium iodide (4-ASP)) allow for the construction of two supramolecular assemblies (*t*Q[14]/2-ASP and *t*Q[14]/4-ASP), which can undergo a reversible exchange under both acidic and neutral conditions and can used for the detection of methyl violet (MV^{2+}, Fig. 22a).[133] As these two supramolecular assemblies have similar properties, only 2-ASP is described here. 2-ASP is protonated to 2-$ASPH^+$ in the Tris-HCl buffer (pH = 2). In addition, it occurs in an unprotonated form at pH = 6. The supramolecular assembly *t*Q[14]/2-$ASPH^+$ resulting from the interaction of 2-$ASPH^+$ with *t*Q[14] exhibits faint fluorescence. In contrast, the assembly *t*Q[14]/2-ASP created from the interaction of unprotonated 2-ASP and *t*Q[14], displays pronounced fluorescence. This fluorescence intensity can be modulated through pH adjustments. A resettable molecular logic gate system was established through deprotonation via acid–base neutralization involving *t*Q[14] and a hemicyanine dye. The signal response of this system can be switched back and forth by successive addition of either H^+ or OH^-, which switches the fluorescence state between "OFF" and "ON." This research has far-reaching implications for the fabrication of molecular INHIBIT logic gates by using twisted Q[*n*]-based supramolecular interactions. Furthermore, the introduction of MV^{2+} to the *t*Q[14]/2-ASP complex led to a total quenching of emission. Therefore, the stimulus-responsive supramolecular assemblies could function as a turn-off fluorescence sensor to detect MV^{2+}. Finally, using this idea, an analytical method for MV^{2+} with a detection limit of 3.2×10^{-7} mol/L was devised.

In Section 4.2, we described that TPAP-Mb@*t*Q[14] responds sensitively and specifically to $Fe(CN)_6^{3-}$ with a lower limit of detection (1.64×10^{-7} M). Recently, our group prepared supramolecular assembly *t*Q[14]-DAAB using *t*Q[14] and *p*-diaminoazobenzene (DAAB) (Fig. 22b).[134] When *t*Q[14]-DAAB is stimulated by anions (F^-, ACO^-, Cl^-, ClO_2^-, SO_4^{2-}, NO_3^-, Br^-, I^-, PF_6^-, $H_2PO_4^-$, ClO_4^-, and HSO_4^-), it exhibits responses to fluoride (F^-) and acetate (ACO^-) in water. The addition of F^- or ACO^- to the *t*Q[14]-DAAB solution causes a colour change, observable to the unaided eye, from orange to yellow and a significant change in the UV–vis spectrum (Fig. 22c). This effect is probably caused by the high negative charge density on the AcO^- and F^- anions, leading to strong hydrogen bonding interactions between them and DAAB, which causes the colour change. Therefore, *t*Q[14]-DAAB supramolecular self-assemblies have the potential to be employed for the development of F^- and ACO^- sensors. Gratifyingly, we successfully obtained a *t*Q[14]-DAAB anion sensor with detection limits of 5.17×10^{-6} M for AcO^- and 2.31×10^{-5} M for F^-.

Fig. 22 a) Binding modes of *t*Q[14] with 2-ASP and illustration of the fluorescence mechanism. Reproduced with permission from ref. 133. Copyright 2017, American Chemical Society; b) Relative UV–vis response of *t*Q[14]-DAAB (2.0×10^{-5} mol/L) in the presence of AcO^- and F^- (100 equiv. of *t*Q[14]-DAAB). (inset) Alteration in colorimetric response following the introduction of 100 equiv. of tetrabutylammonium salt of AcO^- and F^- into Tris-HCl (pH = 3) solutions containing *t*Q[14]-DAAB. Reproduced with permission from ref. 134. Copyright 2022, Wiley-VCH Verlag GmbH & Co. KGaA, Weinheim; c) Illustration of the stimulus response of the

*t*Q[14]-DAAB system. d) Fluorescence images of *t*Q[14]-ThT (50 μM) after the introduction of eight triazole pesticides (50 μM) under UV-lamp irradiation (365 nm). Reproduced under the terms of the CC–BY Creative Commons Attribution 4.0 International License (https://creativecommons.org/licenses/by/4.0/). e) Possible response mechanism for fluorescent probe *t*Q[14]-ThT with flusilazole.

Our group further expanded the use of *t*Q[14]-based sensors for detecting flusilazole, a non-fluorescent triazole fungicide. We allowed the *t*Q[14]-ThT probe to interact with flusilazole and observed sensitive fluorescence quenching with a detection limit of 1.27×10^{-8} mol/L (Fig. 22d).[135] The *t*Q[14]-ThT probe exhibits a specific response to flusilazole because the side cavity of *t*Q[14] contains the dimethylaminophenyl moiety of ThT, which enhances the fluorescence of ThT. The introduction of flusilazole leads to the interaction between the azole moiety of flusilazole and the quaternary ammonium moiety of ThT (Fig. 22e). This interaction diminishes the electron-withdrawing characteristics of the quaternary ammonium moiety, ultimately causing a reduction in the fluorescence emitted by the *t*Q[14]-ThT-flusilazole system.

6.3 Sensors based on *t*Q[15]

In Section 4.3, we describe the APy@*t*Q[15]@Q[10] linear supramolecular polymer. This polymer showed good staining and recognition of cell morphology when applied to HeLa cell imaging, which implies that *t*Q[15] has the potential to be employed for cell staining and recognition.

7. Adsorption and Separation Materials

Adsorptive separation is widely used in the chemical industry. Adsorptive separation is of great significance for the purification of the components of gas or liquid mixtures, advanced processing, and prevention and control of the pollution of wastewater and gas. The cavities of macrocyclic compounds can complex/adsorb guest molecules to separate different substances.[44,45,76,77,79,136–138] Therefore, macrocyclic compounds have been used for separating the lowest-boiling azeotropes, isomers, and pollutants. In particular, Q[*n*]s with their unique pore structures are well suited for use as adsorptive separation materials.[30,76,80] However, most of the existing macrocyclic hosts have only a single cavity of limited size, which may hamper their application. Double-cavity Q[*n*]s with their unique structures are a potentially powerful tool for solving such problems.

7.1 Adsorption and separation materials based on *bis-ns*-Q[10]

Our group reported the use of double-cavity *bis-ns*-Q[10] as an adsorbent material to isolate pyridine (Py).[107] Py could be isolated from toluene (Tol)/Py, benzene (Ben)/Py, or a mixture of Tol/Ben/Py with purity close to 99.9% using *bis-ns*-Q[10]. Fig. 23 shows a schematic diagram of the Py separation and recovery process. When different volumes of the three guests are mixed with *bis-ns*-Q[10], Py is selectively retained in the cavity of *bis-ns*-Q[10] stabilized by C–H···O=C hydrogen bonds between two H atoms of Py and two portal O atoms of *bis-ns*-Q[10], whereas the other guests are rejected. Powder X-ray diffraction and gas chromatography studies have been used to show that *bis-ns*-Q[10] strongly favours the adsorption of Py in contrast to that of

Fig. 23 Illustration of the use of solid *bis-ns*-Q[10] to separate Py from toluene and benzene.

Tol and Ben. *Bis-ns*-Q[10] exhibits excellent reusability, and the guest adsorbed in *bis-ns*-Q[10] can be removed by heating. The separation performance of *bis-ns*-Q[10] does not degrade significantly even after recycling ten times. This process is also feasible in mimic industrial separation. For example, an adequate amount of solid *bis-ns*-Q[10] was added to the mixture of Py/Tol/Ben, which was then stirred for 6 h at room temperature before vacuum adsorption and filtration. The results showed that the content of Ben and Tol increased from 87.67% to 99.93%, while that of Py decreased from 12.33% to 0.07% after the introduction of solid *bis-ns*-Q[10]. Moreover, a semi-permeable stationary phases separation method based on the principle of column chromatography was designed, and good separation results were obtained. The separation process of Py/Tol/Ben by *bis-ns*-Q[10] has the advantages of mild operating conditions and very good separation efficiency. In addition, *bis-ns*-Q[10] can be recycled and reutilized, hence, this is a highly promising material for industrial separation processes.

7.2 Adsorption and separation materials based on *t*Q[14]

The examples above prove that *t*Q[*n*] can be used as an adsorptive separation material. Our group reported an adsorptive separation material for potassium ferricyanide based on a *t*Q[14] supramolecular polymer (TPAP-Mb@*t*Q[14]),[106] which was prepared through the supramolecular self-assembly of *t*Q[14] and a triphenylamine derivative (TPAP-Mb). TPAP-Mb@*t*Q[14] effectively adsorbs and removes $Fe(CN)_6^{3-}$ from aqueous solutions (removal efficiency: 97.38%). In addition, *t*Q[14] is reusable.

Double-cavity Q[*n*]s serve as a distinctive class of separation materials, adept at selectively adsorbing hydrocarbons. The efficiency of hydrocarbon separation is high when there is an optimal size match between the cavities of the double-cavity Q[*n*]s and the guest molecules. Conversely, double-cavity Q[*n*] supramolecular polymers engage in contaminant removal

through electrostatic adsorption, a process whose efficiency is intrinsically linked to the characteristics of these supramolecular polymers. Separation materials derived from double-cavity Q[*n*]s stand out as exceptional adsorbents, holding significant potential for the separation and purification of a diverse array of substances.

8. Supra-amphiphiles

Supra-amphiphiles, which can be small organic molecules or polymers, are amphiphilic molecules formed through non-covalent interactions. Supra-amphiphiles exhibit outstanding control and reversibility. By altering external conditions, their diverse responsiveness can be harnessed to adjust their amphiphilicity in a reversible manner, enabling stimulus-driven assembly and disassembly. Serving as a bridge between colloidal and supramolecular chemistry, supra-amphiphiles play a pivotal role in pioneering new self-assembling functional materials.[29]

8.1 Supra-amphiphiles based on *t*Q[15]

The Huang group harnessed *t*Q[15] and paraquat to establish a host–guest recognition motif in water, subsequently employing it to craft a Ba^{2+}-responsive supra-amphiphile, as depicted in Fig. 24.[139] They initially constructed the novel *t*Q[15]/paraquat molecular recognition motif. Notably, *t*Q[15]/paraquat demonstrated not only robust binding strength in water (K_a = (2.18 ± 0.09) × 10^6 M^{-1}) but also responsiveness to stimulation by metal ions (Ba^{2+}). ^{1}H NMR and UV–vis absorption spectroscopic experiments showed that in this motif, the paraquat binds to *t*Q[15] in a 1:1 molar ratio and is located in the central cavity of *t*Q[15]. The assembly and disassembly of the complex of *t*Q[15]/paraquat can be effectively regulated by the addition and removal of Ba^{2+}. This molecular recognition motif can also be applied to the preparation of barium cation-responsive super-amphiphilic molecules with amphiphilic paraquat derivatives (MV-$C_{11}H_{23}$) as the guest. MV-$C_{11}H_{23}$ contains a hydrophilic 4,4'-bipyridinium unit and hydrophobic alkyl chains. When the concentration of MV-$C_{11}H_{23}$ was higher than its critical aggregation concentration, the amphiphilic MV-$C_{11}H_{23}$ self-assembled into micelles in an aqueous medium, with an average diameter of approximately 6 nm. This diameter was nearly twice as long as that of the MV-$C_{11}H_{23}$ molecule, demonstrating the formation of micelles. When *t*Q[15] was added, the micelles changed into solid nanospheres with an average diameter of 100 nm because of the host–guest complexation. When Ba^{2+} was added, the solid nanospheres again transformed into micelles (average diameter of 10 nm). This study provides a reference for the design and fabrication of supra-amphiphilic molecules based on twisted space capsules. Such a novel recognition motif can be employed for constructing functional structures with a variety of applications.

Fig. 24 Schematic of Ba^{2+}-triggered self-assembly between *t*Q[15] and (MV-$C_{11}H_{23}$).

8.2 Supra-amphiphiles based on Q[6]–Q[7]

The Isaacs group successfully transitioned supramolecular networks to supramolecular polymers using Q[6]–Q[7] heterodimers synthesized from monofunctionalized Q[6] and Q[7] derivatives.[93] They synthesized a hydrophobic guest N1 (Fig. 25) by alkylation of 1,6-hexanediamine with 1-bromooctadecane. The 1,6-hexanediamine moiety of N1 is an excellent guest for both Q[6] and Q[7] cavities in Q[6]–Q[7]. They also prepared the ADA-PEG guest containing hydrophilic PEG tails from adamantane derivatives and PEG derivatives (PEG5000). ADA-PEG with its $AdCH_2NH_2$ binding site can bind to the Q[7] cavity, but not to the Q[6] cavity. These two newly synthesized guests are expected to be combined with Q[6]–Q[7] to prepare supramolecular block copolymers. The ^{1}H NMR spectra showed that Q[6]–Q[7] binds to twice as many equivalents of N1 to produce the hydrophobic homo-assembly Q[6]–Q[7]•$(N1)_2$, while an equimolar mixture of Q[6]–Q[7], ADA-PEG, and N1 self-assembles into the amphiphilic block copolymer N1•Q[6]–Q[7]•ADA-PEG. Dynamic light scattering and scanning electron microscopy results showed that Q[6]–Q[7]•$(N1)_2$ self-assembles into a supramolecular network, which may be due to the physical entanglement of the octadecyl tail of N1 and Q[6]–Q[7] linking the head of 1,6-hexanediamine together. It also showed that N1•Q[6]–Q[7]•ADA-PEG self-assembles to form supramolecular micelles of approximately uniform size, with a diameter of 125 ±7.6 nm. These micelles were assembled with the hydrophobic octadecyl chains of N1 as the core and hydrophilic PEG chains as the crown. Interestingly, the addition of 1 equiv. of ADA-PEG (PEG5000) to Q[6]–Q[7]•$(N1)_2$ results in the transformation of the supramolecular network into supramolecular micelles (diameter: 108 ± 8.9 nm) (Fig. 25). The diameter was smaller probably because excess N1 enters the core structure of the micelle, leading to a tighter alignment of the polymer on the micelle surface. Supramolecular lattices and micelles formed from Q[6]–Q[7] exhibit pronounced stimuli-responsiveness. Consequently, the capacity to modulate the morphology of double-cavity Q[*n*] supramolecular block copolymers and to engineer functional structures offers a useful reference for advanced biological and technological applications.

Fig. 25 Transformation of supramolecular networks into supramolecular micelles.

9. Inert Components

Although the widespread use of pesticides has greatly increased agricultural production, it has also caused serious harm to humans and the environment. Therefore, the use of "green" pesticides, which exhibit reduced toxicity toward human beings and cause less environmental pollution, is attracting increasing research interest. One potential strategy for mitigating the associated risks of pesticide application is through their encapsulation. *t*Q[14] can encapsulate Hymexazol (**HMI**) to form a host–guest complex and enhances its ability to inhibit the growth of a phytopathogenic fungus, namely *Botrytis cinerea* Pers.[104] Our group investigated the host–guest inclusion of Q[*n*]s (Q[7], hemimethyl-substituted cucurbit[6]uril (HHMeQ[6]), and *t*Q[14]) with **HMI** and found that **HMI** forms a 1:1 inclusion complex with Q[*n*] with a moderate binding constant and binds inside the cavity of Q[*n*]. We evaluated the inhibition activity of **HMI** and **HMI**@Q[*n*] inclusion complexes against *Botrytis cinerea* Pers. using the mycelial growth rate method (Fig. 26). The experimental results showed that **HMI**@Q[*n*] was more effective in inhibiting the bacterial growth than uncomplexed **HMI**. Notably, when the *n*(**HMI**):*n*(*t*Q[*n*]) ratios were 1:1 and 1:2, the **HMI**@*t*Q[14]-inhibition rates were 84.8% and 87.5%, respectively. However, there was no change in the inhibition effect after the interaction of β-cyclodextrin and **HMI**. The reason for the improved inhibitory effect of the Q[*n*]s and their mechanism of action are presently unknown. The encapsulation of these Q[*n*]s offers a promising approach for enhancing the fungicidal effect of **HMI** and reducing the environmental burden of synthetic agrochemicals.

Fig. 26 Comparison of the antibacterial effects of **HMI** and **HMI**@Q[*n*]. Reproduced with permission from ref. 104. Copyright 2018, Wiley-VCH Verlag GmbH & Co. KGaA, Weinheim.

10. Summary and Outlook

This review summarizes all the research progress dating back from the discovery of double-cavity Q[*n*]s to the present day, including their synthesis, structures, properties, and applications. As of now, double-cavity Q[*n*]s, with their sophisticated design and innovative properties, have carved out significant roles in areas such as polymer science, supramolecular chemistry, biology, and materials research.

Double-cavity Q[*n*]s have many advantages and broad application prospects over the traditional single-cavity Q[*n*]s. Firstly, double-cavity Q[*n*]s with their flexible structure can be flexibly deformed according to the shape of the guest to allow for a wider range of encapsulation compared to that achieved using traditional single-cavity Q[*n*]s. Secondly, *t*Q[*n*]s from the family of double-cavity Q[*n*]s can be solubilized more extensively in both water and organic solvents compared to traditional single-cavity Q[*n*]s. Thirdly, *t*Q[*n*]s and (±)-AGD of the double-cavity Q[*n*] family exhibit chirality. However, there are still some aspects of double-cavity Q[*n*]s that are yet to be explored.

(1) Resolution of the enantiomers of double-cavity Q[*n*]s. Separating the enantiomers of double-cavity Q[*n*]s presents an intriguing challenge. Their chirality paves the way for groundbreaking developments in the realm of Q[*n*]s. Yet, the act of distinguishing and isolating these chiral enantiomers has proven to be quite daunting. Successfully isolating either the left- or right-spinning double-cavity Q[*n*]s will not only validate their chirality but also catalyze the creation of additional chiral materials centered around them—marking a significant milestone for Q[*n*]s. An innovative approach might involve the separation of chiral double-cavity Q[*n*]s via host–guest interactions, specifically between the chiral guest and the double-cavity Q[*n*]s. Leveraging these chiral double-cavity Q[*n*]s with distinct left and right spins could lead to the synthesis of pioneering materials, resulting in potentially groundbreaking research findings.

(2) Supramolecular self-assembly and framework construction. Supramolecular self-assembly is a bottom-up approach to craft functional materials featuring diverse structures. It not only bridges the gap between microscopic molecules and macroscopic materials but also imparts distinctive properties to the resulting materials. Strategies to prepare supramolecular membranes, supramolecular networks, or supramolecular polymers using well-designed guests with supramolecular self-assembly and frameworks of double-cavity Q[*n*]s may move double-cavity Q[*n*]s toward practical applications.

(3) Bionic materials. Double-cavity Q[*n*]s are universally soluble in aqueous environments, and *t*Q[*n*]s can even be dissolved in organic solvents, which is a natural advantage for making biomimetic materials that mimic the natural world. How to endow materials of double-cavity Q[*n*]s with the ability to mimic biological behaviour such as stimulus response, luminescence, drug transport and release, and energy storage will be a persistent and difficult challenge. If the structural adaptability and special properties of the host–guest combination of the double-cavity Q[*n*]s are fully utilized in material design, the resulting materials will have a significantly optimized bionic effect.

(4) Adsorption and separation materials. While double-cavity Q[*n*]s have already demonstrated success in adsorption and separation, there is a pressing need to further develop and refine adsorption and separation materials centered on these Q[*n*]s. This urgency stems from the substantial energy demands associated with extracting high-purity compounds from chemical mixtures—an inherently energy-intensive endeavor. The size and shape of the compound to be separated determines to some extent whether it can be encapsulated and thus separated. Double-cavity Q[*n*]s with a figure-of-eight shape, due to their structural flexibility, may adapt appropriately to match the size and shape of guests, potentially offering

distinctive advantages in the separation of mixtures and demonstrating prospective applicability.

(5) Modification of double-cavity Q[*n*]s. Double-cavity Q[*n*]s boast numerous benefits. Enhanced recognition of guest molecules can be achieved by tailoring double-cavity Q[*n*]s to have congruent dimensions and specialized complexation sites, paving the way for novel application areas. While there's a proposed method to incorporate *bis*-*ns*-Q[10] with functional segments, its universal application to all double-cavity Q[*n*]s is hindered due to the inherent stability. An alternative pathway might involve crafting modified double-cavity Q[*n*]s via the polymerization of adapted glycoluril monomers. In addition, the introduction of hydroxyl groups on double-cavity Q[*n*]s in the presence of hydrogen peroxide and UV light is a viable option.

In essence, while the journey of crafting materials centered on double-cavity Q[*n*]s presents its set of challenges, the vast potential they harbor undeniably signals a plethora of research opportunities in associated domains.

Author Contributions

Qing Li: conceptualization, funding acquisition, supervision, and writing – review and editing; Zhengwei Yu: drawing the figures and tables, and drafting the manuscript; Carl Redshaw: review and editing; Xin Xiao: resources and giving suggestions; Zhu Tao: visualization and supervision descriptions.

Conflicts of Interest

There are no conflicts of interest to declare.

Acknowledgments

This work was supported by the Natural Science Special of Guizhou University (no. (2021)37 Special Post B) and the National Natural Science Foundation of China (No. 22361011). C.R. thanks the University of Hull for financial support.

References

1 J.-M. Lehn, *Angew. Chem., Int. Ed.*, 1988, **27**, 89–112.
2 C. Rest, R. Kandanelli and G. Fernandez, *Chem. Soc. Rev.*, 2015, **44**, 2543–2572.
3 A. Kumar, S.-S. Sun and A. J. Lees, *Coord. Chem. Rev.*, 2008, **252**, 922–939.
4 Y. Sasaki, X. Lyu, W. Tang, H. Wu and T. Minami, *Bull. Chem. Soc. Jpn.*, 2021, **94**, 2613–2622.
5 L. L. Lock, Y. Li, X. Mao, H. Chen, V. Staedtke, R. Bai, W. Ma, R. Lin, Y. Li, G. Liu and H. Cui, *ACS Nano*, 2017, **11**, 797–805.
6 J. Tian, P. K. Thallapally and B. P. McGrail, *Supramol. Chem.*, 2012, DOI: 10.1002/9780470661345.smc127.
7 D. Wu, P.-F. Zhang, G.-P. Yang, L. Hou, W.-Y. Zhang, Y.-F. Han, P. Liu and Y.-Y. Wang, *Coord. Chem. Rev.*, 2021, **434**, 213709.
8 C. J. Bruns and J. F. Stoddart, *Nat. Nanotechnol.*, 2013, **8**, 9–10.
9 X. Liang, L. Li, J. Tang, M. Komiyama and K. Ariga, *Bull. Chem. Soc. Jpn.*, 2020, **93**, 581–603.
10 R. Dong, Y. Zhou, X. Huang, X. Zhu, Y. Lu and J. Shen, *Adv. Mater.*, 2015, **27**, 498–526.
11 C. J. Pedersen, *Science*, 1988, **241**, 536–540.
12 J. S. Bradshaw and R. M. Izatt, *Acc. Chem. Res.*, 1997, **30**, 338–345.
13 G. W. Gokel, W. M. Leevy and M. E. Weber, *Chem. Rev.*, 2004, **104**, 2723–2750.
14 Y. Yang, T. Zhao, M.-H. Li, X. Wu, M. Han, S.-C. Yang, Q. Xu, L. Xian, X. Chi, N.-J. Zhao, H. Cui, S. Li, J.-S. Hu, B. Zhang and Y. Jiang, *Chem. Eng. J.*, 2023, **451**, 138962.
15 X. Ji, H. Wang, Y. Li, D. Xia, H. Li, G. Tang, J. L. Sessler and F. Huang, *Chem. Sci.*, 2016, **7**, 6006–6014.
16 K. Yang, S. Qi, X. Yu, B. Bai, X. Zhang, Z. Mao, F. Huang and G. Yu, *Angew. Chem., Int. Ed.*, 2022, **61**, e202203786.
17 A. R. Hedges, *Chem. Rev.*, 1998, **98**, 2035–2044.
18 A. Harada, Y. Takashima and H. Yamaguchi, *Chem. Soc. Rev.*, 2009, **38**, 875–882.
19 H. L. Sun, Y. Chen, J. Zhao and Y. Liu, *Angew. Chem., Int. Ed.*, 2015, **54**, 9376–9380.
20 E. M. M. Del Valle, *Process Biochem.*, 2004, **39**, 1033–1046.
21 S. B. Nimse and T. Kim, *Chem. Soc. Rev.*, 2013, **42**, 366–386.
22 S. E. Matthews and P. D. Beer, *Supramol. Chem.*, 2005, **17**, 411–435.
23 D.-S. Guo and Y. Liu, *Chem. Soc. Rev.*, 2012, **41**, 5907–5921.
24 Y. Wu, Z. Ma, J. Shi, X. Sun, K. Yang and Z.-Y. Li, *Chin. Chem. Lett.*, 2022, **33**, 5116–5119.
25 K. Kim, N. Selvapalam, Y. H. Ko, K. M. Park, D. Kim and J. Kim, *Chem. Soc. Rev.*, 2007, **36**, 267–279.
26 C. Marquez, R. R. Hudgins and W. M. Nau, *J. Am. Chem. Soc.*, 2004, **126**, 5806–5816.
27 O. A. Geras'ko, D. G. Samsonenko and V. P. Fedin, *Russ. Chem. Rev.*, 2002, **71**, 741–760.
28 X. Du, X. Liu, H. Su, X. Cheng, L. Li, H. Gu, X. Xing, D. Qiu and H. Hao, *Microchem. J.*, 2022, **182,** 107942.
29 X. Zhang and C. Wang, *Chem. Soc. Rev.*, 2011, **40**, 94–101.
30 X. L. Ni, X. Xiao, H. Cong, L. L. Liang, K. Cheng, X. J. Cheng, N. N. Ji, Q. J. Zhu, S. F. Xue and Z. Tao, *Chem. Soc. Rev.*, 2013, **42**, 9480–9508.
31 H. Wang, Y. Fan, Y. Hou, B. Chen, J. Lei, S. Yu, X. Chen and X. Hou, *Nat. Commun.*, 2022, **13**, 1906.
32 Y. Zhou, K. Jie, R. Zhao and F. Huang, *J. Am. Chem. Soc.*, 2019, **141**, 11847–11851.
33 K. Jie, Y. Zhou, E. Li and F. Huang, *Acc. Chem. Res.*, 2018, **51**, 2064–2072.
34 M. Xue, Y. Yang, X. Chi, Z. Zhang and F. Huang, *Acc. Chem. Res.*, 2012, **45**, 1294–1308.
35 J.-F. Chen, Q. Lin, Y.-M. Zhang, H. Yao and T.-B. Wei, *Chem. Commun.*, 2017, **53**, 13296–13311.
36 L. Chen, Y. Cai, W. Feng and L. Yuan, *Chem. Commun.*, 2019, **55**, 7883–7898.
37 M. Bojtár, J. Kozma, Z. Szakács, D. Hessz, M. Kubinyi and I. Bitter, *Sens. Actuators B Chem.*, 2017, **248**, 305–310.
38 H. Chen, X. Jia and C. Li, *Chin. J. Chem.*, 2015, **33**, 343–345.
39 R.-L. Lin, R. Li, H. Shi, K. Zhang, D. Meng, W.-Q. Sun, K. Chen and J.-X. Liu, *J. Org. Chem.*, 2020, **85**, 3568–3575.

40 J. Zhou, G. Yu and F. Huang, *Chem. Soc. Rev.*, 2017, **46**, 7021–7053.
41 Z. Zheng, W.-C. Geng, Z. Xu and D.-S. Guo, *Isr. J. Chem.*, 2019, **59**, 913–927.
42 Q. Duan, Y. Cao, Y. Li, X. Hu, T. Xiao, C. Lin, Y. Pan and L. Wang, *J. Am. Chem. Soc.*, 2013, **135**, 10542–10549.
43 R. Oun, R. S. Floriano, L. Isaacs, E. G. Rowan and N. J. Wheate, *Toxicol. Res.*, 2014, **3**, 447–455.
44 L.-L. Tan, H. Li, Y. Tao, S. X. Zhang, B. Wang and Y.-W. Yang, *Adv. Mater.*, 2014, **26**, 7027–7031.
45 G. Zhang, B. Hua, A. Dey, M. Ghosh, B. A. Moosa and N. M. Khashab, *Acc. Chem. Res.*, 2021, **54**, 155–168.
46 J. Liang, S. Xing, P. Brandt, A. Nuhnen, C. Schlüsener, Y. Sun and C. Janiak, *J. Mater. Chem. A*, 2020, **8**, 19799–19804.
47 P. Wang, Y. Wu, Y. Zhao, Y. Yu, M. Zhang and L. Cao, *Chem. Commun.*, 2017, **53**, 5503–5506.
48 H. Li, Y. Yang, F. Xu, T. Liang, H. Wen and W. Tian, *Chem. Commun.*, 2019, **55**, 271–285.
49 Y. Liu, H. Yang, Z. Wang and X. Zhang, *Chem. - Asian J.*, 2013, **8**, 1626–1632.
50 Z. Gao, J. Zhang, N. Sun, Y. Huang, Z. Tao, X. Xiao and J. Jiang, *Org. Chem. Front.*, 2016, **3**, 1144–1148.
51 J. Kim, I.-S. Jung, S.-Y. Kim, E. Lee, J.-K. Kang, S. Sakamoto, K. Yamaguchi and K. Kim, *J. Am. Chem. Soc.*, 2000, **122**, 540–541.
52 Z. Duan, F. Xu, X. Huang, Y. Qian, H. Li and W. Tian, *Macromol. Rapid Commun.*, 2022, **43**, 2100775.
53 A. Harada, A. Hashidzume and Y. Takashima, *Adv. Polym. Sci.,* 2006, **201**, 1–43.
54 Z. Y. Li, Y. Zhang, C. W. Zhang, L. J. Chen, C. Wang, H. Tan, Y. Yu, X. Li and H. B. Yang, *J. Am. Chem. Soc.*, 2014, **136**, 8577–8589.
55 L. Isaacs, *Acc. Chem. Res.*, 2014, **47**, 2052–2062.
56 R. Behrend, E. Meyer and F. Rusche, *Justus Liebigs Ann. Chem.*, 1905, **339**, 1–37.
57 W. A. Freeman, W. L. Mock and N. Y. Shih, *J. Am. Chem. Soc.*, 1981, **103**, 7367–7368.
58 L. Isaacs, *Isr. J. Chem.*, 2011, **51**, 578–591.
59 A. Day, A. P. Arnold, R. J. Blanch and B. Snushall, *J. Org. Chem.*, 2001, **66**, 8094–8100.
60 A. I. Day, R. J. Blanch, A. P. Arnold, S. Lorenzo, G. R. Lewis and I. Dance, *Angew. Chem., Int. Ed.* , 2002, **41**, 275–277.
61 S. Liu, P. Y. Zavalij and L. Isaacs, *J. Am. Chem. Soc.*, 2005, **127**, 16798–16799.
62 K. I. Assaf and W. M. Nau, *Chem. Soc. Rev.*, 2015, **44**, 394–418.
63 S. J. Barrow, S. Kasera, M. J. Rowland, J. del Barrio and O. A. Scherman, *Chem. Rev.*, 2015, **115**, 12320–12406.
64 S. Liu, C. Ruspic, P. Mukhopadhyay, S. Chakrabarti, P. Y. Zavalij and L. Isaacs, *J. Am. Chem. Soc.*, 2005, **127**, 15959–15967.
65 W. L. Mock and N.-Y. Shih, *J. Org. Chem.*, 1986, **51**, 4440–4446.
66 W. S. Jeon, K. Moon, S. H. Park, H. Chun, Y. H. Ko, J. Y. Lee, E. S. Lee, S. Samal, N. Selvapalam, M. V. Rekharsky, V. Sindelar, D. Sobransingh, Y. Inoue, A. E. Kaifer and K. Kim, *J. Am. Chem. Soc.*, 2005, **127**, 12984–12989.
67 M. V. Rekharsky, T. Mori, C. Yang, Y. H. Ko, N. Selvapalam, H. Kim, D. Sobransingh, A. E. Kaifer, S. Liu, L. Isaacs, W. Chen, S. Moghaddam, M. K. Gilson, K. Kim and Y. Inoue, *Proc. Natl. Acad. Sci. U. S. A.*, 2007, **104**, 20737–20742.
68 J. Pennakalathil, E. Jahja, E. S. Ozdemir, O. Konu and D. Tuncel, *Biomacromolecules*, 2014, **15**, 3366–3374.
69 L. Liu, *J. Inclusion Phenom. Macrocyclic Chem.*, 2016, **87**, 1–12.
70 J. Murray, K. Kim, T. Ogoshi, W. Yao and B. C. Gibb, *Chem. Soc. Rev.*, 2017, **46**, 2479–2496.
71 K. Kim, *Chem. Soc. Rev.*, 2002, **31**, 96–107.
72 N. J. Wheate and C. Limantoro, *Supramol. Chem.*, 2016, **28**, 849–856.
73 S. Walker, R. Oun, F. J. McInnes and N. J. Wheate, *Isr. J. Chem.*, 2011, **51**, 616–624.
74 J. Liu, C. S. Y. Tan and O. A. Scherman, *Angew. Chem., Int. Ed.*, 2018, **57**, 8854–8858.
75 S. Dong, B. Zheng, F. Wang and F. Huang, *Acc. Chem. Res.*, 2014, **47**, 1982–1994.
76 X. Yang, C. Li, M. Giorgi, D. Siri, X. Bugaut, B. Chatelet, D. Gigmes, M. Yemloul, V. Hornebecq, A. Kermagoret, S. Brasselet, A. Martinez and D. Bardelang, *Angew. Chem., Int. Ed.*, 2022, **61**, e202214039.
77 M. Liu, R. Cen, J. Zhao, Z.-C. Yu, L.-X. Chen, Q. Li, Z. Tao and X. Xiao, *Sep. Purif. Technol.*, 2023, **304**, 122342.
78 R. X. Cheng, F. Y. Tian, Y. Q. Zhang, K. Chen, Q. J. Zhu and Z. Tao, *J. Mater. Sci.*, 2020, **55**, 16497–16509.
79 S. Pan, R. Saha, S. Mandal, S. Mondal, A. Gupta, M. A. Fernández-Herrera, G. Merino and P. K. Chattaraj, *J. Phys. Chem. C*, 2016, **120**, 13911–13921.
80 X. Li, X. Xie, H. Luo, L. Li, Z. Li, Z. Xue and W. Li, *J. Colloid Interface Sci.*, 2017, **498**, 31–46.
81 J. D. Barrio, J. Liu, R. A. Brady, C. S. Y. Tan, S. Chiodini, M. Ricci, R. Fernandez-Leiro, C.-J. Tsai, P. Vasileiadi, L. Di Michele, D. Lairez, C. Toprakcioglu and O. A. Scherman, *J. Am. Chem. Soc.*, 2019, **141**, 14021–14025.
82 H. Chen, Y. Chen, H. Wu, J.-F. Xu, Z. Sun and X. Zhang, *Biomaterials*, 2018, **178**, 697–705.
83 Y. Liu, Z. Huang, X. Tan, Z. Wang and X. Zhang, *Chem. Commun.*, 2013, **49**, 5766–5768.
84 Z. Wang, C. Sun, K. Yang, X. Chen and R. Wang, *Angew. Chem., Int. Ed.*, 2022, **61**, e202206763.
85 H.-J. Kim, D. R. Whang, J. Gierschner and S. Y. Park, *Angew. Chem., Int. Ed.*, 2016, **55**, 15915–15919.
86 G. Ghale and W. M. Nau, *Acc. Chem. Res.*, 2014, **47**, 2150–2159.
87 M. Nilam, S. Karmacharya, W. M. Nau and A. Hennig, *Angew. Chem., Int. Ed.*, 2022, **61**, e202207950.
88 S. Sinn and F. Biedermann, *Isr. J. Chem.*, 2018, **58**, 357–412.
89 W.-H. Huang, S. Liu, P. Y. Zavalij and L. Isaacs, *J. Am. Chem. Soc.*, 2006, **128**, 14744–14745.
90 J. B. Wittenberg, M. G. Costales, P. Y. Zavalij and L. Isaacs, *Chem. Commun.*, 2011, **47**, 9420–9422.
91 W.-H. Huang, P. Y. Zavalij and L. Isaacs, *Org. Lett.*, 2009, **11**, 3918–3921.
92 J. B. Wittenberg, P. Y. Zavalij and L. Isaacs, *Angew. Chem., Int. Ed.*, 2013, **52**, 3690–3694.
93 M. Zhang, L. Cao and L. Isaacs, *Chem. Commun.*, 2014, **50**, 14756–14759.
94 Q. Li, S.-C. Qiu, J. Zhang, K. Chen, Y. Huang, X. Xiao, Y. Zhang, F. Li, Y.-Q. Zhang, S.-F. Xue, Q.-J. Zhu, Z. Tao, L. F. Lindoy and G. Wei, *Org. Lett.*, 2016, **18**, 4020–4023.
95 X.-J. Cheng, L.-L. Liang, K. Chen, N.-N. Ji, X. Xiao, J.-X. Zhang, Y.-Q. Zhang, S.-F. Xue, Q.-J. Zhu, X.-L. Ni and Z. Tao, *Angew. Chem., Int. Ed.*, 2013, **52**, 7252–7255.

96 M. I. El-Barghouthi, H. M. Abdel-Halim, F. J. Haj-Ibrahim, K. Bodoor and K. I. Assaf, *J. Inclusion Phenom. Macrocyclic Chem.*, 2015, **82**, 323–333.

97 B. Vinciguerra, L. Cao, J. R. Cannon, P. Y. Zavalij, C. Fenselau and L. Isaacs, *J. Am. Chem. Soc.*, 2012, **134**, 13133–13140.

98 D. Lucas, T. Minami, G. Iannuzzi, L. Cao, J. B. Wittenberg, P. Anzenbacher, Jr. and L. Isaacs, *J. Am. Chem. Soc.*, 2011, **133**, 17966–17976.

99 L. Cao and L. Isaacs, *Org. Lett.*, 2012, **14**, 3072–3075.

100 Q. Li, S.-C. Qiu, K. Chen, Y. Zhang, R. Wang, Y. Huang, Z. Tao, Q.-J. Zhu and J.-X. Liu, *Chem. Commun.*, 2016, **52**, 2589–2592.

101 C.-H. Wang, Q. Tang, J. Zhang, Y.-Q. Yao, X. Xiao, Y. Huang and Z. Tao, *New J. Chem.*, 2018, **42**, 9244–9251.

102 J. Zhang, Q. Tang, Z. Z. Gao, S. C. Qiu, Y. Huang and Z. Tao, *Chem. - Eur. J.*, 2017, **23**, 10092–10099.

103 J. Zhang, Y.-Y. Xi, Q. Li, Q. Tang, R. Wang, Y. Huang, Z. Tao, S.-F. Xue, L. F. Lindoy and G. Wei, *Chem. - Asian J.*, 2016, **11**, 2250–2254.

104 Y. Fan, R.-H. Gao, X. Xiao and Z. Tao, *Isr. J. Chem.*, 2018, **58**, 466–471.

105 R. Nally and L. Isaacs, *Tetrahedron*, 2009, **65**, 7249–7258.

106 W. Zhang, Y. Luo, P.-H. Zhu, X.-L. Ni, C. Redshaw, Z. Tao and X. Xiao, *ACS Appl. Mater. Interfaces*, 2022, **14**, 37068–37075.

107 M. Liu, R. Cen, J. Li, Q. Li, Z. Tao, X. Xiao and L. Isaacs, *Angew. Chem., Int. Ed.*, 2022, **61**, e202207209.

108 Q. Liu, Q. Li, X.-J. Cheng, Y.-Y. Xi, B. Xiao, X. Xiao, Q. Tang, Y. Huang, Z. Tao, S.-F. Xue, Q.-J. Zhu and J.-X. Zhang, *Chem. Commun.*, 2015, **51**, 9999–10001.

109 V. Lemaur, G. Carroy, F. Poussigue, F. Chirot, J. De Winter, L. Isaacs, P. Dugourd, J. Cornil and P. Gerbaux, *ChemPlusChem*, 2013, **78**, 959–969.

110 G. Carroy, V. Lemaur, J. De Winter, L. Isaacs, E. De Pauw, J. Cornil and P. Gerbaux, *Phys. Chem. Chem. Phys.*, 2016, **18**, 12557–12568.

111 S.-C. Qiu, K. Chen, Y. Wang, Z.-Y. Hua, F. Li, Y. Huang, Z. Tao, Y.-J. Zhang and G. Wei, *Inorg. Chem. Commun.*, 2017, **86**, 49–53.

112 Y. Yang, X.-L. Ni, J.-F. Xu and X. Zhang, *Chem. Commun.*, 2019, **55**, 13836–13839.

113 R. Nally, O. A. Scherman and L. Isaacs, *Supramol. Chem.*, 2010, **22**, 683–690.

114 E. A. Appel, J. del Barrio, J. Dyson, L. Isaacs and O. A. Scherman, *Chem. Sci.*, 2012, **3**, 2278.

115 K. M. Park, J. H. Roh, G. Sung, J. Murray and K. Kim, *Chem. - Asian J.*, 2017, **12**, 1461–1464.

116 P.-Q. Zhang, Q. Li, Z.-K. Wang, Q.-X. Tang, P.-P. Liu, W.-H. Li, G.-Y. Yang, B. Yang, D. Ma and Z.-T. Li, *Chin. Chem. Lett.*, 2023, **34**, 107632.

117 W. Zhang, Y. Luo, J. Zhao, C. Zhang, X.-L. Ni, Z. Tao and X. Xiao, *Chin. Chem. Lett.*, 2022, **33**, 2455–2458.

118 Y. Luo, W. Zhang, M. X. Yang, X. H. Feng, C. Redshaw, Q. Li, Z. Tao and X. Xiao, *Macromolecules*, 2022, **55**, 1642–1646.

119 W. Zhang, Y. Luo, X.-L. Ni, Z. Tao and X. Xiao, *Chem. Eng. J.*, 2022, **446**, 136954.

120 Y. Luo, W. Zhang, Q. Ren, Z. Tao and X. Xiao, *ACS Appl. Mater. Interfaces*, 2022, **14**, 29806–29812.

121 W. Zhang, Y. Luo, M.-H. Jia, X.-L. Ni, Z. Tao, C.-D. Xiao and X. Xiao, *Sens. Actuators*, *B*, 2022, **366**, 132006.

122 J. B. Wittenberg and L. Isaacs, *Supramol. Chem.*, 2014, **26**, 157–167.

123 H. N. Kim, W. X. Ren, J. S. Kim and J. Yoon, *Chem. Soc. Rev.*, 2012, **41**, 3210–3244.

124 Z. Xu, J. Yoon and D. R. Spring, *Chem. Soc. Rev.*, 2010, **39**, 1996–2006.

125 X. Chen, T. Pradhan, F. Wang, J. S. Kim and J. Yoon, *Chem. Rev.*, 2012, **112**, 1910–1956.

126 K. P. Carter, A. M. Young and A. E. Palmer, *Chem. Rev.*, 2014, **114**, 4564–4601.

127 S. K. Sahoo, D. Sharma, R. K. Bera, G. Crisponi and J. F. Callan, *Chem. Soc. Rev.*, 2012, **41**, 7195–7227.

128 F. Zhang, Y. Sun, D. Tian, W. S. Shin, J. S. Kim and H. Li, *Chem. Commun.*, 2016, **52**, 12685–12693.

129 T. Shukla, A. K. Dwivedi, R. Arumugaperumal, C.-M. Lin, S.-Y. Chen and H.-C. Lin, *Dyes Pigm.*, 2016, **131**, 49–59.

130 X. Zhang, W. Wu, Z. Tao and X.-L. Ni, *Beilstein J. Org. Chem.*, 2019, **15**, 1705–1711.

131 R. Cen, M. Liu, H. Xiao, H.-P. Yang, L.-X. Chen, Q. Li, C.-H. Wang, Z. Tao and X. Xiao, *Sens. Actuators*, *B*, 2023, **378**, 133126.

132 W. Zhang, Y. Luo, M.-X. Yang, W.-H. Lin, C. Redshaw, X.-L. Ni, Y. Huang, Z. Tao and X. Xiao, *Microchem. J.*, 2022, **178**, 107364.

133 J. Zhang, Q. Tang, Z.-Z. Gao, Y. Huang, X. Xiao and Z. Tao, *J. Phys. Chem. C*, 2017, **121**, 11119–11123.

134 C.-h. Wang, Q. Tang, J. Zhao, X. Xiao, Z. Tao and Y. Huang, *ChemistrySelect* 2022, **7**, e202202843.

135 Y. Fan, R.-H. Gao, Y. Huang, B. Bian, Z. Tao and X. Xiao, *Front. Chem.*, 2019, **7**, 154–161.

136 Q. Li, K. Jie and F. Huang, *Angew. Chem., Int. Ed.*, 2020, **59**, 5355–5358.

137 K. Jie, M. Liu, Y. Zhou, M. A. Little, S. Bonakala, S. Y. Chong, A. Stephenson, L. Chen, F. Huang and A. I. Cooper, *J. Am. Chem. Soc.*, 2017, **139**, 2908–2911.

138 Z.-Q. Wang, X. Wang and Y.-W. Yang, *Adv. Mater.*, 2023, 2301721.

139 Q. Li, J. Sun, J. Zhou, B. Hua, L. Shao and F. Huang, *Org. Chem. Front.*, 2018, **5**, 1940–1944.

Zhengwei Yu

Zhengwei Yu was born in China in 1996. He obtained his BS degree from Guizhou University, China, in 2019. In 2021, he joined the laboratory of Qing Li at Guizhou University to pursue his Master's degree in Chemistry. His current research is focused on the properties and applications of Q[*n*]s.

Qing Li

Qing Li obtained her Master's degree at Guizhou University, China, under the supervision of Prof. Zhu Tao. Then, she joined the laboratory of Prof. Feihe Huang at Zhejiang University, China, and obtained her PhD in Supramolecular Chemistry in 2021. She was a visiting student in Prof. Sébastien Perrier's group at Warwick University, England (September 2019 to March 2020). Currently, she is working at Guizhou University. Her current research interests are focused on responsive self-assembly, supramolecular assemblies, and functional materials based on host–guest chemistry.

Carl Redshaw

Carl Redshaw is Chair of Inorganic Materials at the University of Hull, UK. His research interests include macrocyclic chemistry, including calixarenes and cucurbiturils, coordination chemistry, catalysis, and metal-based imaging and anti-cancer compounds.

Xin Xiao

Xin Xiao received his PhD from the University of Science & Technology, Beijing (USTB), in 2015. He is a professor of chemistry at Guizhou University, China. His research is focused on the cucurbit[*n*]uril-based coordination chemistry.

Zhu Tao

Zhu Tao received his PhD from the University of New South Wales, Australia, in 2001. He is a professor of chemistry at Guizhou University, China. His research concerns cucurbit[*n*]uril-based supramolecular chemistry.

Graphical Abstract: